Nonlinear Transport Behavior of Low Dimensional Electron Systems

by

JingQiao Zhang

A dissertation submitted to the Graduate Faculty in Physics in partial fulfillment of the requirements for the degree of Doctor of Philosophy,The City University of New York.

2009

© 2009

JingQiao Zhang

All Rights Reserved

This manuscript has been read and accepted for the Graduate Faculty in Physics in satisfaction of the dissertation requirement for the degree of Doctor of Philosophy.

September 18, 2008	Sergey A. Vitkalov
	Chair of Examining Committee
September 18, 2008	Steven Greenbaum
Date	Executive Officer
	Frederick W. Smith
	David Schmeltzer
	Jiu-Feng Tu
	Lev Deych
	Supervisory Committee

THE CITY UNIVERSITY OF NEW YORK

Abstract

Nonlinear Transport Behavior of Low Dimensional Electron Systems

by

JingQiao Zhang

Thesis Advisor: Professor Sergey Vitkalov

The nonlinear behavior of low-dimensional electron systems attracts a great deal of attention for its fundamental interest as well as for potentially important applications in nanoelectronics. In response to microwave radiation and *dc* bias, strongly nonlinear electron transport that gives rise to unusual electron states has been reported in two-dimensional systems of electrons in high magnetic fields. There has also been great interest in the nonlinear response of quantum ballistic constrictions, where the effects of quantum interference, spatial dispersion and electron-electron interactions play crucial roles.

In this thesis, experimental results of the research of low dimensional electron gas systems are presented. The first nonlinear phenomena were observed in samples of highly mobile two dimensional electrons in GaAs heavily doped quantum wells at different magnitudes of DC and AC (10 KHz to 20 GHz) excitations. We found that in the DC excitation regime the differential resistance oscillates with the DC current

and external magnetic field, similar behavior was observed earlier in AlGaAs/GaAs heterostructures[C.L. Yang *et al*]. At external AC excitations the resistance is found to be also oscillating as a function of the magnetic field. However the form of the oscillations is considerably different from the DC case. We show that at frequencies below 100 KHz the difference is a result of a specific average of the DC differential resistance during the period of the external AC excitations.

Secondly, in similar samples, strong suppression of the resistance by the electric field is observed in magnetic fields at which the Landau quantization of electron motion occurs. The phenomenon survives at high temperatures at which the Shubnikov de Haas oscillations are absent. The scale of the electric fields essential for the effect, is found to be proportional to temperature in the low temperature limit. We suggest that the strong reduction of the longitudinal resistance is a result of a nontrivial distribution function of the electrons induced by the DC electric field. We compare our results with a theory proposed recently. The comparison allows us to find the quantum scattering time of 2D electron gas at high temperatures, in a regime, where previous methods were not successful.

In addition, we observed a zero differential resistance state (ZDRS) in response to a direct current above a threshold value $I > I_{th}$ applied to a two-dimensional system of electrons at low temperatures in a strong magnetic field. Entry into the ZDRS, which is not observable above several Kelvins, is accompanied by a sharp dip in the differential resistance. Additional analysis reveals instability of the electrons

for $I > I_{th}$ and an inhomogeneous, non-stationary pattern of the electric current. We suggest that the dominant mechanism leading to the new electron state is the redistribution of electrons in energy space induced by the direct current.

Finally, we present the results of rectification of microwave radiation generated by an asymmetric, ballistic dot at different frequencies (1-40GHz), temperatures (0.3K-6K) and magnetic fields. A strong reduction of the microwave rectification is found in magnetic fields at which the cyclotron radius of electron orbits at the Fermi level is smaller than the size of the dot. With respect to the magnetic field, both symmetric and anti-symmetric contributions to the directed transport are presented in this thesis. The symmetric part of the rectified voltage changes significantly with microwave frequency ω at $\omega\tau_f \geq 1$, where τ_f is the time of a ballistic electron flight across the dot. The results lead consistently toward the ballistic origin of the effect, and can be explained by the strong nonlocal electron response to the microwave electric field, which affects both the speed and the direction of the electron motion inside the dot.

Dedication to

my most dearest mom, dad, and Migly

Acknowledgments

First, I wish to express my appreciation to my supervisor Prof. Sergey Vitkalov. With his guidance, help and patience throughout my research work, I have learned a great deal and grown up on the track of physical science. He is a great role model for me as a physicist. His solid background and experience in physics, his patience and strictness, even his humor were engraved in my heart and will inspire me in the future.

I would also like to thank all the people in the Sarachik group. The group leader, Myriam Sarachik, a distinguished professor of CUNY, has helped us enormously. Her passion for physics and her personality enlighten all physics students at CCNY including me. The former and current members of her group, Kevin Mertes,Yoko Suzuki, Yeekin Tsui, Kurt James and Sean McHugh have always been a great source of advice and help..

I am also grateful to Professor David Schmeltzer and his student Husan-Yeh Chang. They have been very generous spending time discussing physics and have provided many useful suggestions. Their supportive help is not just limited to my study.

I would also like to thank Professor Frederick Smith. I took his classes in the beginning of my Ph.D. program. He is very kind to every student. I appreciate his great patience in correcting my English in my homework assignments. Since he introduced me to my advisor, Prof. Vitkalov, I started my own research career.

I would also like to thank Professor Jiufeng Tu, who gave me the opportunity to present my work to his group. This experience greatly helped me in improving my presentation skills.

I must also thank the former students of Professor Maksee, Ping Wang and Chaoming Song, two very smart young men. They helped me a lot in my study. We shared a lot of great time and because of them my life in New York is richer.

I would also like to thank Natalia Romero, my colleague and another student of Prof. Sergey Vitkalov. She helped me a lot. We have a great time working in the lab.

I would also like to thank all the members of my thesis committee, Sergey Vitkalov, David Schmeltzer, Frederick W. Smith, Lev Deych and Jiu-Feng Tu for taking the time to read my thesis. I would like to thank Joe Birman, Timothy Boyer and V.P. Nair for their wonderful lectures in physical science.

Lastly and mostly, I would like to thank my parents and my Migly, they have always been supporting me with their unlimited and selfless love. They have always believed in me unconditionally and never questioned my decisions. They are my soul. Without them, I could not have finished this Long March. The only words I can say are "I love you all!"

Thank you all again!

终于可以在毕业论文上写下感谢的话语！

为了这个代表知识和智慧的物理学哲学博士学位，整整走过十一个春秋。付出的不只是艰辛，承受的不只是挫折。十一年来，默默地接受命运的安排而无法抗争，流泪地面对生离死别而无力阻止，只有心中的那个目标是明确的，不灭的。支持我义无反顾地迈向目标的源动力是来自我最深爱的妈妈、爸爸和朱格丽的无私和无限的支持。每一次在迷茫和困难的面前，总是想起他们鼓励和殷切的目光，更想起为了实现这个目标，已经付出的无法承受的代价，这是一条已经没有后路的道路。为了这个目标，父亲离开的时候，我不在他身边；朱格丽走的时候，我不在她左右。留给我的是永不磨灭的思念、心灵上的伤痕、遗憾和懊丧！只有在睡梦中，才能重温一家团圆的幸福时光，然而醒来的时候，是无数次满脸泪水，心里空空地面对残酷地现实世界，简简单单的亲人团聚对于我却是不可及的奢望！而荣耀到来的时候，一家人却不能够共同分享，就像那亏缺的月亮，冷冷地挂在夜空。只有妈妈，我如今唯一的心灵支柱见证这一历史时刻。

这份荣得但还到的荣誉不属于我的，而是属于我永远深爱的，而同时也深爱我的爸爸，妈妈和家乾的！

生活中这沉重的一页终于可以翻过去了！心里对未来充满了期待！

爸、妈、味，我爱你们！

CONTENTS

LIST OF FIGURES

1. INTRODUCTION

Solid materials can be classified into three categories: insulators, semiconductors and metals. This classification scheme is based on the conducting properties of the materials. The conductivity of charge carriers in a solid provides a clear criterion to distinguish between the different types of solids. We can also view these different types of solids in terms of their different band structures. In the case of a metal the conductance band is partially filled. In the case of an insulator, the conductance band is empty. In a semiconductor there is a small energy gap so that at a finite temperature a small density of electrons will be excited into the conductance band. A direct way to investigate the transport behavior of a conducting solid material is by applying an electric field to excite the systems and observing the response. This is the primary method employed in our experiments described in this thesis.

1.1 Linear Response of Electrons to Electric Field

1.1.1 Drude Model

The Drude model gives us a simple theory of metallic conduction. It was put forth by P. Drude in the beginning of the 20th century. It is a very successful model and we still

use it today as a quick practical way to roughly estimate the transport properties of electrons and generate a comprehensive picture for many new complicated theoretical models.

Electrical Conductivity of a Metal

The conductivity σ is defined by the relation between the current density $\mathbf{j} = -ne\mathbf{v}$ and the electric field $\mathbf{E}$ which induces this current density [1],

$$\mathbf{j} = \sigma\mathbf{E} \tag{1.1}$$

where n is electron density, e is electric charge, $\mathbf{v}$ is the average velocity of the electrons. In the presence of a field $\mathbf{E}$ there will be a mean electronic velocity directed opposite the field, this velocity is given by[1]

$$\mathbf{v} = -\frac{e\mathbf{E}\tau_{\mathrm{tr}}}{m} \tag{1.2}$$

where m is electron mass, τ_{tr} is the relaxation time or the collision time which describes the probability of an electron collision during time dt, $P \sim dt/\tau_{\mathrm{tr}}$. The Drude model gives therefore the following expression for the conductivity

$$\sigma = \frac{ne^2\tau_{\mathrm{tr}}}{m} \tag{1.3}$$

This result follows directly from Newton's equation for an electron in the presence of an electric field $\mathbf{E}$ assuming the relaxation of the electron momentum $\mathbf{p}$[1],

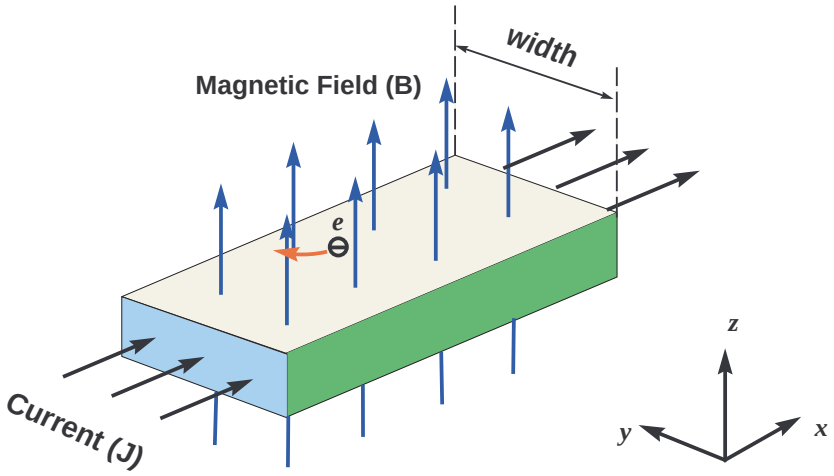

Fig. 1.1: Schematic view of Hall's experiment. If an electric current flows through a conductor in a magnetic field, the magnetic field exerts a transverse force on the moving charge carriers and push the carriers to one side of the conductor.

$$\frac{d\mathbf{p}\,(t)}{dt} = -\frac{\mathbf{p}\,(t)}{\tau_{\mathrm{tr}}} + \mathbf{f}\,(t) \tag{1.4}$$

Hall Effect and Longitudinal Magnetoresistance

The Drude model also describes electron conductivity in the presence of a magnetic field. Due to the Lorentz force $\mathbf{F_L} = -e\,(\mathbf{E} + \mathbf{v} \times \mathbf{H}/c)$, the conductivity acquires a non-diagonal component inducing the Hall effect . Hall's experiment is depicted in Fig. 1.1. An electric field E_x is applied to a slab metal extending in the x-direction. A current density j_x is driven by the electric field $\mathbf{E}$. The magnetic field $\mathbf{H}$ is applied in the positive z-direction. In the presence of a magnetic field, $\mathbf{B}$ Eq. 1.4 for the

electron momentum becomes[1]

$$\frac{d\mathbf{p}}{dt} = -e\left(\mathbf{E} + \frac{\mathbf{p}}{mc} \times \mathbf{H}\right) - \frac{\mathbf{p}}{\tau_{\mathrm{tr}}} \tag{1.5}$$

the solution of Eq. 1.5 provides the resistivity tensor[2]:

$$\begin{pmatrix} E_x \\ E_y \end{pmatrix} = \begin{bmatrix} \rho_{xx} & \rho_{xy} \\ \rho_{yx} & \rho_{yy} \end{bmatrix} \begin{pmatrix} J_x \\ J_y \end{pmatrix} \tag{1.6}$$

and

$$\rho_{xx} = \sigma^{-1} = m/ne^2\tau_{tr} \tag{1.7}$$

$$\rho_{yx} = -\rho_{xy} = H/|e|n_s \tag{1.8}$$

where $n_s = n/d$ and d is thickness of the slab.

1.1.2 Electron transport in metals: The Boltzmann equation

The Boltzmann equation describes the electron transport in a more complete fashion, taking into account possible space and time variations of the electron density and the external electric and magnetic fields. The equation describes the time evolution of the distribution function of electrons $f(\mathbf{k})$ [3],

$$\partial f(\mathbf{k})/\partial t + \dot{\mathbf{k}} \cdot \frac{\partial f(\mathbf{k})}{\partial \mathbf{k}} + \mathbf{v}_{\mathbf{k}} \cdot \nabla f(\mathbf{k}) = \left.\frac{\partial f(\mathbf{k})}{\partial t}\right]_{\mathrm{coll.}} \tag{1.9}$$

where, the first term in the left side, $\partial f/\partial t$ represents the net rate of change of the distribution function. It will be zero in the so-called steady state. The distribution changes due to the external fields at a rate given by the term $\dot{\mathbf{k}} \cdot \frac{\partial f(\mathbf{k})}{\partial \mathbf{k}}$. The rate of change of the distribution due to the diffusion of carriers is given by the term, $\mathbf{v_k} \cdot \nabla f(\mathbf{k})$. The distribution function f changes at a rate $\frac{\partial f(\mathbf{k})}{\partial t}\Big\rfloor_{\text{coll.}}$ due to the effect of scattering.

At steady state, the Boltzmann equation includes three types of effects which change the distribution function $f(\mathbf{k})$: (a) diffusion moves carriers in and out of the region $\mathbf{r}$, (b) change of the $\mathbf{k}$ vector of each carrier as a result of an external field and (c) scattering (or collision) of the carriers. In a steady state, the net rate of change of $f(\mathbf{k})$ is zero.

The collision integral $\frac{\partial f}{\partial t}\rfloor_{\text{coll.}}$ is often used in the so-called τ approximation[3]

$$\frac{df\left(\mathbf{k}\right)}{dt}\Big\rfloor_{\text{coll.}} = -\frac{f\left(\mathbf{k}\right) - f_0\left(\mathbf{k}\right)}{\tau} \tag{1.10}$$

where τ denotes the relaxation time. In a spatially uniform and stationary case Eq. 1.9 reads[3]

$$\left(-\frac{\partial f_0}{\partial \varepsilon}\right) \mathbf{v_k} \cdot e\mathbf{E} = -\frac{\partial f(\mathbf{k})}{\partial t}\Big\rfloor_{\text{coll.}}. \tag{1.11}$$

The current density is defined by

$$\mathbf{J} = \frac{-e}{4\pi^3} \int \mathbf{v_k} f(\mathbf{k}) d\mathbf{k}. \tag{1.12}$$

The Eq. 1.10, Eq. 1.11 and Eq. 1.12 give the electric current[3]:

$$\mathbf{J} = -\frac{e^2}{4\pi^3}\int \tau \mathbf{v_k}\left(\mathbf{v_k}\cdot\mathbf{E}\right)\left(-\frac{\partial f_0}{\partial \varepsilon}\right)d\mathbf{k}. \tag{1.13}$$

This result can be written as $\mathbf{j} = \sigma\mathbf{E}$, where the conductivity tensor σ is

$$\sigma = -\frac{e^2}{4\pi^3}\int \tau \mathbf{v_k}\mathbf{v_k}\left(-\frac{\partial f_0}{\partial \varepsilon}\right)d\mathbf{k}. \tag{1.14}$$

The result above shows that only electrons near the Fermi surface provide significant contributions to the conductivity because of the step-function character of f_0.

1.2 Transport in a quantized magnetic field: Two-dimensional Electron Gas

In a bulk metal, electronic motion is free in all three spatial dimensions. If the electronic motion in one dimension is restricted, the electrons can only move on a two dimensional plane. Most of the recent work has been done on the GaAs-AlGaAs heterojunctions, in which a thin two-dimensional conducting layer is formed at the interface between GaAs and AlGaAs.

The following picture [2] Fig. 1.2 shows the typical structure of a 2DEG. The Fermi energy, E_F, in the wide gap AlGaAs layer is higher than in the narrow gap GaAs layer. Consequently electrons spill over from the AlGaAs leaving behind positively charged donors. The space change gives rise to an electrostatic potential that causes

the bands to bend as shown. At equilibrium the Fermi energy is constant across the sample. The electron density is sharply peaked near the GaAs-AlGaAs interface (at the interface the Fermi energy is inside the bended conduction band) forming a 2D conducting layer. The electron motion perpendicular the surface is quantized, forming 2D sub bands. The carrier concentration in a 2DEG typically ranges from $2\times10^{11}\,\mathrm{cm}^2$ to $2\times10^{12}\,\mathrm{cm}^2$.

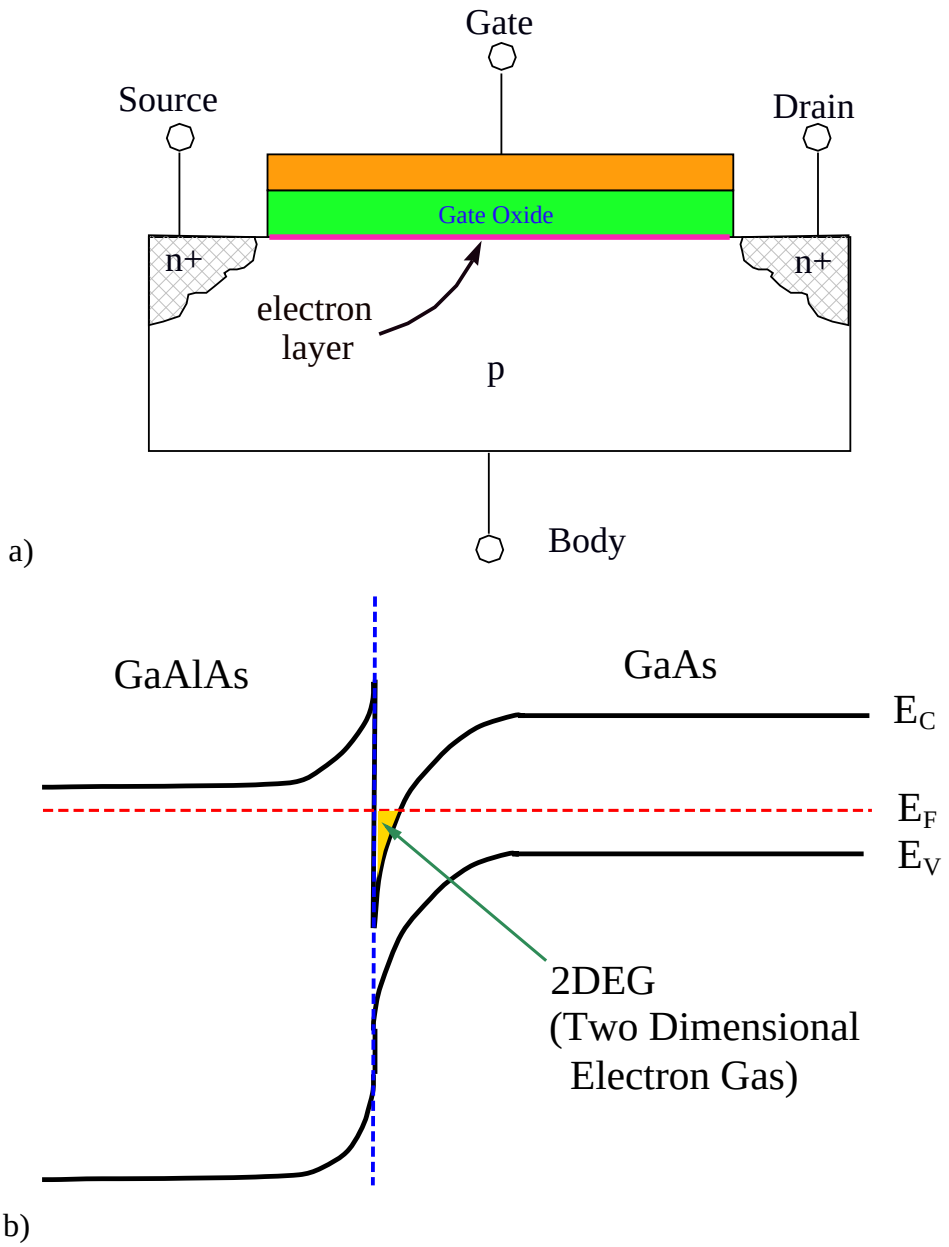

Fig. 1.2: a) The profile of typical CMOS device. In MOSFETs, the 2DEG is only present when the transistor is in inversion mode, and is found directly beneath the gate oxide. b) Energy Band of typical heterostructure.

1.2.1 The energy band and density of states of 2DEG.

The 2D electron eigenfunctions normalized to an area S can be written in the form [2]

$$\Psi(x,y) = \frac{1}{\sqrt{S}} \exp(ik_x x) \exp(ik_y y) \tag{1.15}$$

with the energies given by[2]

$$E = E_s + \frac{\hbar^2}{2m}\left(k_x^2 + k_y^2\right) \tag{1.16}$$

E_s is counted from the bottom of conduction band or higher electron sub-band formed due to the quantization of the electron motion in the z direction. At zero magnetic field the density of electron states per unit area is given by[2]

$$N(E) \equiv \frac{1}{S}\frac{d}{dE} N_T(E) = \frac{m}{\pi\hbar^2}\theta(E - E_s), \tag{1.17}$$

where N_T is total number of electron states below the energy E. At high magnetic fields the lateral motion of the 2D electrons is quantized. L. D. Landau has theoretically predicted the quantization. Assuming a constant magnetic field $\mathbf{B}$ in the direction perpendicular to the plane of a 2D conductor, the vector potential is taken as $\mathbf{A} = -\hat{x}By$. The electron wave function is $\Psi(x,y) = \frac{1}{\sqrt{L}} \exp[ikx]\,\chi(y)$. The Schördinger equation for the transverse function $\chi(y)$ has the following form [2]

$$\left[E_s + \frac{p_y^2}{2m} + \frac{1}{2}m\omega_c^2 \left(y + y_k\right)^2\right] \chi\left(y\right) = E\chi\left(y\right) \tag{1.18}$$

where E_s is the ω_c is the cyclotron frequency and $y_k \equiv \dfrac{\hbar k}{eB}$. The eigenfunctions of the equation are Hermite functions with eigenvalues[2]:

$$E\left(n,k\right) = E_s + \left(n + \frac{1}{2}\right)\hbar\omega, \;\; n = 0, 1, 2... \tag{1.19}$$

This discrete spectrum makes the density of states of the 2DEG, $N_s\left(E\right)$ (Eq. 1.17), break up into a sequence of peaks spaced by $\hbar\omega_c$ (neglecting Zeeman splitting)[2].

$$N_s\left(E,B\right) \approx \frac{2eB}{h}\sum_{n=0}^{\infty}\delta\left[E - E_s - \left(n + \frac{1}{2}\right)\hbar\omega_c\right] \tag{1.20}$$

This is illustrated in Fig. 1.3. Without the scattering, the spikes are δ functions. But, in practice, the scattering processes spread them out in energy.

As we change the magnetic field B, the energies of the Landau levels are changed in accordance with Eq. 1.20. The resistivity ρ_{xx} oscillates as Landau levels cross the Fermi energy (see Fig. 1.3) . At small magnetic fields the quantum oscillations decay due to temperature smearing and the finite width of the Landau levels [4].

1.3 Nonlinear Magneto-Transport in High Mobility 2DEG

Recent experiments have discovered new transport phenomena in a high-mobility two-dimensional electron gas in GaAs/AlGaAs heterostructures.

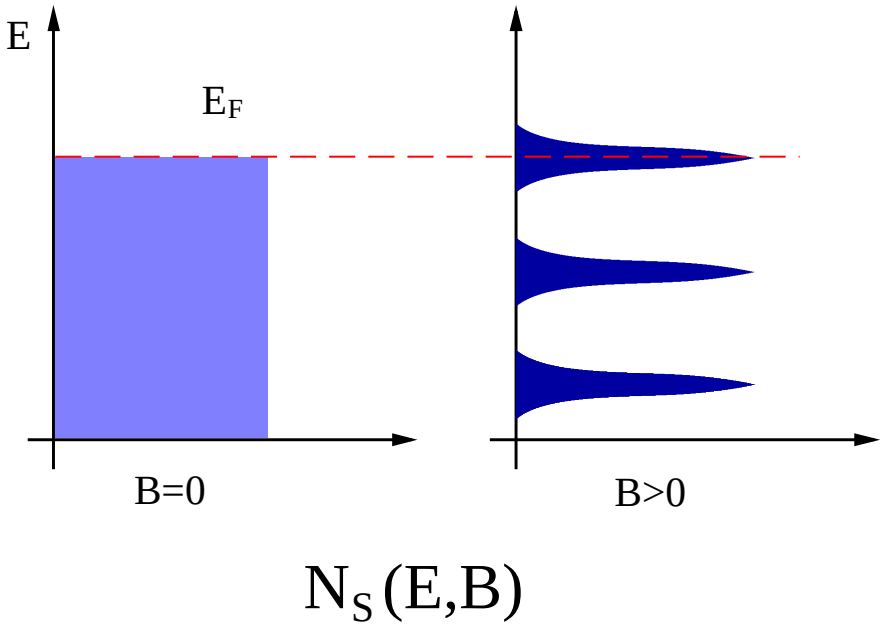

Fig. 1.3: The density of states at a zero magnetic field is constant and electrons fill up the states up to the Fermi surface. At a non-zero magnetic field, the DOS is a sequence of peaks in energy space

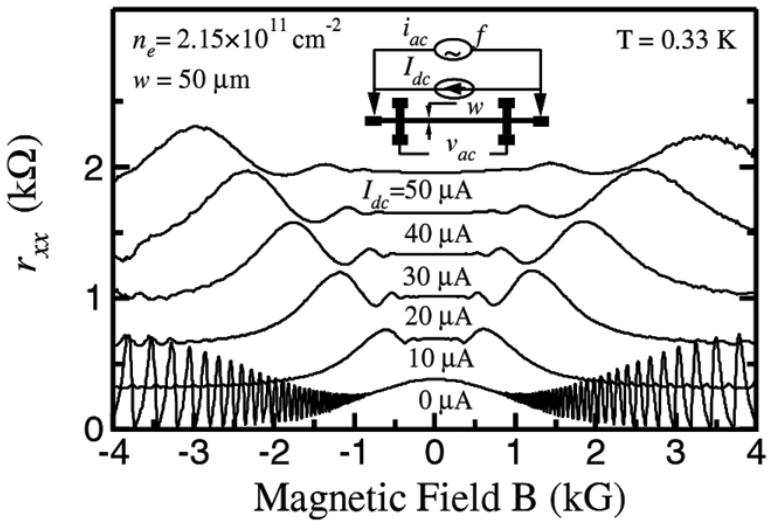

Fig. 1.4: The measured differential magnetoresistance traces at various dc currents I_{dc} for C. L. Yang's sample which is a high mobility one. The oscillations are roughly periodic in 1/B and appear at a weak magnetic field. As the DC current is increased, the peaks of the oscillations move toward a higher field position.

1.3.1 Landau-Zener Tunneling Between Landau Orbits

In one of the experiments [5] a remarkable oscillation effect is observed in the magnetoresistance of a high-mobility 2DEG at a weak magnetic field. At this field, the Shubnikov-de Haas oscillations are not observable in the linear response. In the nonlinear response, a different type of oscillations of the longitudinal resistance r_{xx} are observed at different current applied to the 2DEG. These oscillations are roughly periodic in $1/B$. The oscillation period depends on the DC bias J_{dc}. This is shown in Fig. 1.4[5].

These oscillations have been interpreted as Landau-Zener transitions of 2D electrons between Landau levels during impurity scattering. When a current density J is

directed along a 2DEG Hall bar placed in a classically strong ($\omega_c\tau_{tr} \gg 1$) magnetic field B normal to the 2D plane, an electric field E_y appears along the transverse direction of the Hall bar due the Hall effect, $E_y = v_d B$, where v_d is drift velocity in crossed electric and magnetic field.

According to the above discussion, the spectrum of the 2DEG is quantized into a series of Landau levels with a wave function, $\Psi(x,y) = \frac{1}{\sqrt{L}} \exp[ikx]\, \chi_n(y - y_k)$, where n is the Landau level index and $\chi_n(y - y_k)$ is the Hermite wave function centered at $y_k = \dfrac{\hbar k}{eB}$.

The energy levels are given by [5]

$$E_{ny} = \left(n + \frac{1}{2}\right)\hbar\omega_c - eE_y y_k + \frac{1}{2}mv_d^2 \tag{1.21}$$

from Eq. 1.21, we can see that the Landau levels are tilted spatially along the y direction with a slope eE_y (Fig.1.5).

The Fermi level is also tilted along the y direction due to the independence of the electron density n on y [5]. When elastic scattering of an electron occurs, this electron may hop from an occupied level to an empty level (a Landau-Zener transition). The transition shifts the guiding center y_k of the electron. The hopping distance (shift) is

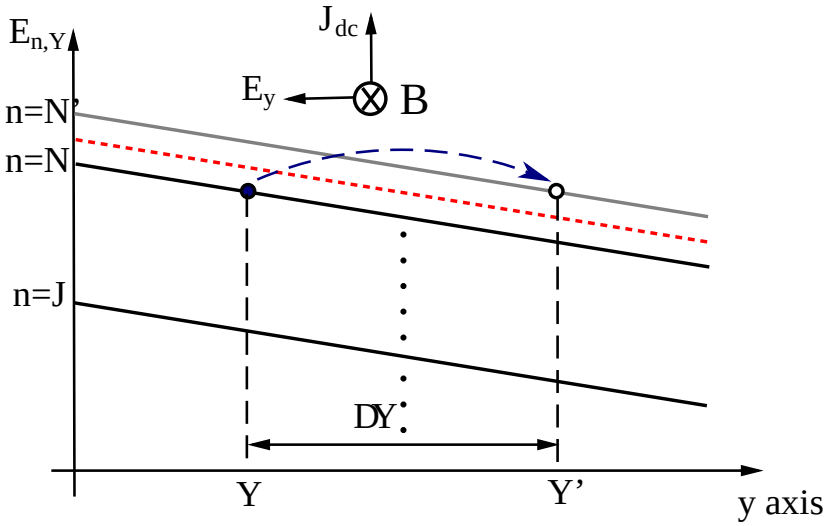

Fig. 1.5: The Landau levels are spatially tilted along the direction of the electric field (y direction), and the Fermi level has the same slope as the Landau levels. Elastic scattering leads to electrons hopping between different Landau levels with a distance given by $\Delta Y = Y' - Y \approx 2R_c$

determined by[5]

$$\begin{aligned} \Delta y &= y_k - y_k' \\ &= \frac{l\hbar\omega_c}{eE_y} \\ &= \gamma R_c \approx 2R_c. \end{aligned} \tag{1.22}$$

The hopping of electrons described above changes the longitudinal conductivity of the 2DEG. The variation of conductivity was observed in the experiment [5].

1.3.2 Nonlinear Transport Induced by AC/DC Excitation and Proposed Theory due to Inelastic Scattering

Recent experiments have also discovered strong magneto-oscillations governed by microwave radiation[6]. Subsequent works [7], [8], [9] done at a high radiation power have demonstrated that the minimum of the resistivity oscillations evolve into zero-resistance state (ZRS). Recent theoretical study [10] has proposed that these magneto-oscillations are due to a change of the electron distribution function, induced by the external excitation. This theory is important for the experiments presented in this thesis.

The longitudinal conductivity can be expressed by[10]

$$\sigma_{xx} = \int d\varepsilon \sigma_{dc}(\varepsilon) \left[-\partial_\varepsilon f(\varepsilon)\right] \tag{1.23}$$

where $f(\varepsilon)$ is the electron distribution function and $\sigma_{dc}(\varepsilon)$ determines the contribution of electrons with energy ε to the dissipative transport. For a classically strong magnetic field, $\omega_c \tau_{\rm tr} \gg 1$, the σ_{dc} reduces to [11] [12]

$$\sigma_{dc}(\varepsilon) = \sigma_{dc}^D \tilde{\nu}^2(\varepsilon) \tag{1.24}$$

where $\sigma_{dc}^D = e^2 \nu_0 v_F^2 / 2\omega_c^2 \tau_{\rm tr}$ is the dc Drude conductivity per spin in a magnetic field. $\tilde{\nu}(\varepsilon) = \nu(\varepsilon)/\nu_0$ is the normalized dimensionless density of states, $\nu(\varepsilon)$ is the DOS in a magnetic field B and $\nu_0 = m/2\pi$ is the DOS at zero B ($\hbar = 1$). At a stationary state

the scattering rate equation for the non-equilibrium distribution function $f(\varepsilon)$ reads [10]

$$\frac{f(\varepsilon)-f_0(\varepsilon)}{\tau_{\rm in}} = E_\omega^2 \frac{\sigma_\omega^D}{2\omega^2\nu_0}\sum_{\pm}\tilde{\nu}(\varepsilon\pm\omega)[f(\varepsilon\pm\omega)-f(\omega)] + E_{dc}^2\frac{\sigma_{dc}^D}{\nu_0\tilde{\nu}(\varepsilon)}\partial_\varepsilon[\nu^2(\varepsilon)\partial_\varepsilon f(\varepsilon)] \tag{1.25}$$

where f_0 is Fermi-Dirac distribution function. E_ω and E_{dc} are the magnitudes of the ac and dc electric fields. The first term in the right hand side describes the absorption and emission of the microwave. The second term accounts for the effect of the *dc* electric field. These terms describe the spectral diffusion of electrons in ε-space. The left-hand side accounts for the inelastic relaxation from the non-equilibrium distribution $f(\varepsilon)$ to the thermal equilibrium distribution $f_0(\varepsilon)$. The inelastic collision integral is taken in the τ approximation, with an inelastic relaxation rate $1/\tau_{in}$.

Eq. 1.25 is solved for low magnetic fields, at which the Landau Levels overlap and the DOS is given by

$$\tilde{\nu} = 1 - 2\delta\cos\left(\frac{2\pi\varepsilon}{\omega_c}\right),\ \delta = \exp\left(-\frac{\pi}{\omega_c\tau_q}\right) \tag{1.26}$$

where τ_q is the quantum relaxation time. The analytical solution of f in first order δ may be obtained by introducing the following dimensionless parameters describing

the ac and dc fields:

$$P_\omega = \frac{\tau_{\rm in}}{\tau_{\rm tr}} \left(\frac{eE_\omega v_F}{\omega}\right)^2 \frac{\omega_c^2+\omega^2}{\left(\omega^2-\omega_c^2\right)^2}$$
$$Q_{dc} = \frac{2\tau_{\rm in}}{\tau_{\rm tr}} \left(\frac{eE_{dc} v_F}{\omega_c}\right)^2 \left(\frac{\pi}{\omega_c}\right)^2. \tag{1.27}$$

The solution is

$$f - f_0 = \delta \frac{\omega_c}{2\pi} \frac{\partial f_0}{\partial \varepsilon} \sin\frac{2\pi\varepsilon}{\omega_c} \frac{P_\omega \frac{2\pi\omega}{\omega_c} \sin\frac{2\pi\omega}{\omega_c} + 4Q_{dc}}{1 + P_\omega \sin^2\frac{\pi\omega}{\omega_c} + Q_{de}}. \tag{1.28}$$

This result shows that the oscillations of the DOS induce an oscillatory contribution to the f_0, as depicted in Fig. 1.6.

Although the DOS makes a weak correction to f_0, the term $\partial_\varepsilon f(\varepsilon)$ in Eq. 1.23 can have a strong effect on the conductivity. Assuming the bath temperature T is much larger than the Dingle temperature $T \gg 1/2\pi\tau_q$, then the oscillatory conductivity is

$$\frac{\sigma_{xx}}{\sigma_{dc}^D} = 1 + 2\delta^2 \left[1 - \frac{P_\omega \frac{2\pi\omega}{\omega_c} \sin\frac{2\pi\omega}{\omega_c} + 4Q_{dc}}{1 + P_\omega \sin^2\frac{\pi\omega}{\omega_c} + Q_{de}}\right]. \tag{1.29}$$

Eq. 1.29 includes nonlinear effects both in ac and dc electric fields.

The inelastic relaxation time $\tau_{\rm in}$ is an important parameter. In accordance with Eq. 1.27 and Eq. 1.29, the inelastic scattering determines the nonlinearity of the electron transport. The T dependence of $\tau_{\rm in}$ is of particular importance since it determines the temperature dependence of the nonlinear conductivity σ_{xx}. At not too high T, the

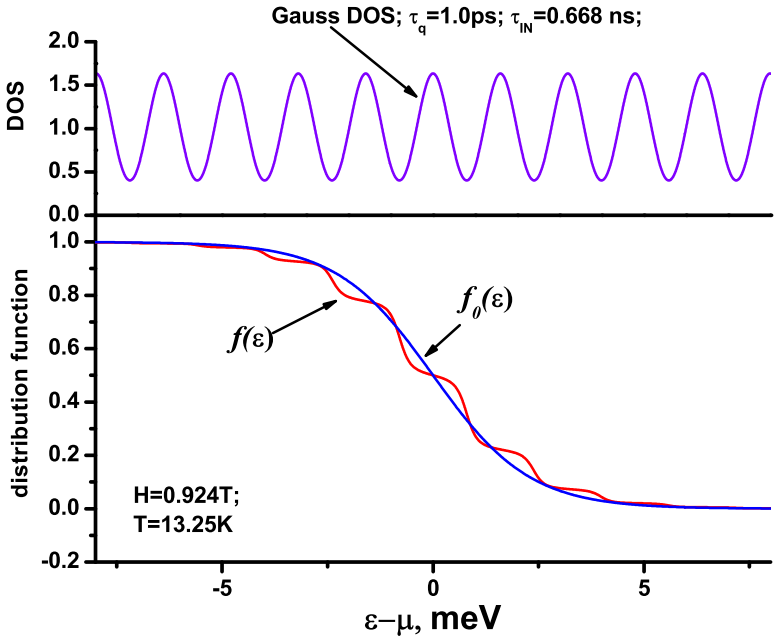

Fig. 1.6: In the upper part of the figure the density of states in the presence of a magnetic field is plotted. A cosine function was used to formulate the oscillatory part of the DOS. In the lower part of the figure, the smooth solid line represents the equilibrium distribution function at a high temperature. The oscillatory solid line is the oscillatory non-equilibrium distribution function excited by a DC fields.

dominant mechanism of inelastic scattering, due to electron-electron collisions[10], leads to the relaxation of the oscillatory term $(f - f_0)$. Under this condition, the T behavior of σ_{xx} is well determined. Under an appropriate approximation , the theory predicts different $\tau_{\rm in}$ for different forms of the DOS[10]

$$\begin{aligned}
\tau_{\rm in}^{-1} &= \frac{\pi T^2 + \varepsilon^2}{4\pi\varepsilon_F} \ln \frac{\kappa v_F}{\omega_c(\omega_c\tau_{\rm tr})^{1/2}}, \text{ Overlapping Landau levels} \\
\tau_{\rm in}^{-1} &\sim \frac{\omega_c}{\Gamma}\frac{T^2 + (\varepsilon/\pi)^2}{\varepsilon_F} \ln \frac{\kappa v_F \tau_q^{1/2}}{\omega_c \tau_{\rm tr}^{1/2}}, \text{ Separated Landau levels.}
\end{aligned} \tag{1.30}$$

Both cases have similar temperature dependence while the characteristic energies are $\varepsilon \sim T$. These theoretical results show that the nonlinear response scales as T^{-2}.

1.4 Motivation

The study of electron transport in low dimensional electron systems reveals a rich variety of nonlinear properties of electron transport. The nonlinear properties of low dimensional systems are subject of strong fundamental interest as well as of paramount importance for practical applications. The majority of contemporary electronic devices are based on implementations of the nonlinear properties of low dimensional materials. Novel and unknown mechanisms of nonlinearity in low dimensional electron systems are targets of the fundamental research presented in this thesis.

2. EXPERIMENTAL TECHNIQUES

This section describes the techniques and procedures used in our experiments.

2.1 The Low Temperature Refrigerator

Most of the fundamental properties of electron materials are obtained at low temperatures. This is because at higher temperatures microscopic randomness tends to mask or even suppress considerably electron propagation through a solid. Moreover at high temperatures inelastic electron relaxation is fast, making nonlinear response of electron systems small. Thus, low temperatures facilitate the study of nonlinear electron transport. In the following part, the low temperature apparatus will be described in detail.

^3He System

A ^3He evaporation cryostat is used in our experiments to reach temperatures below 1K. We have designed and assembled the cryostat in our lab. The home-made cryostat is presented in Fig. 2.1. In order to liquefy the ^3He gas, a regular ^4He refrigerator is used to cool down a 1K-plate. The 1K-plate is soldered to a spiral copper pumping

line. At operating conditions the plate produces temperatures of $T \approx 2$K. This temperature is low enough to liquefy the ^3He gas. The low temperature part of the ^3He container is attached to the 1K-plate with a solid thermal connection. The 2K cold plate is also used as a 2K heat sink preventing nearly all external heat coming into the ^3He pot. All tubes and wires connected to the ^3He pot are thermally anchored to it. The 1K-plate and the ^3He pot are soldered with hard and soft soldering in accordance to the required applications. The soft soldering is much simpler for assembling purposes, whereas the hard soldering gives stronger durability of the apparatus. The ^3He refrigerator is vacuum sealed at low temperatures by using silicon grease on the IVC(inner vacuum chamber) cone. The ^3He refrigerator contains two parts: ^3He pot and sorption (charcoal) pump. The sample is mounted on the ^3He pot. The ^3He pot is made of oxygen free copper and has a 5.2 cm^3 internal volume. These low temperature components are located inside an IVC. In our setup, the sample is in a vacuum and isolated from the refrigerant. The significant advantage of this design is that the system has better temperature control and very small loss of ^3He gas.

Below we describe the operation of the cryostat. ^4He liquid, boiling under standard atmospheric pressure at 4.2K, surrounds the IVC. Inside the IVC there are a 1K-plate and a ^3He pot suspended on stainless steel tubes with thin walls to minimize thermal flows. A capillary dips inside the bath with liquid Helium. An external mechanical pump pumps the liquid ^4He through the capillary in the spiral copper line and cools

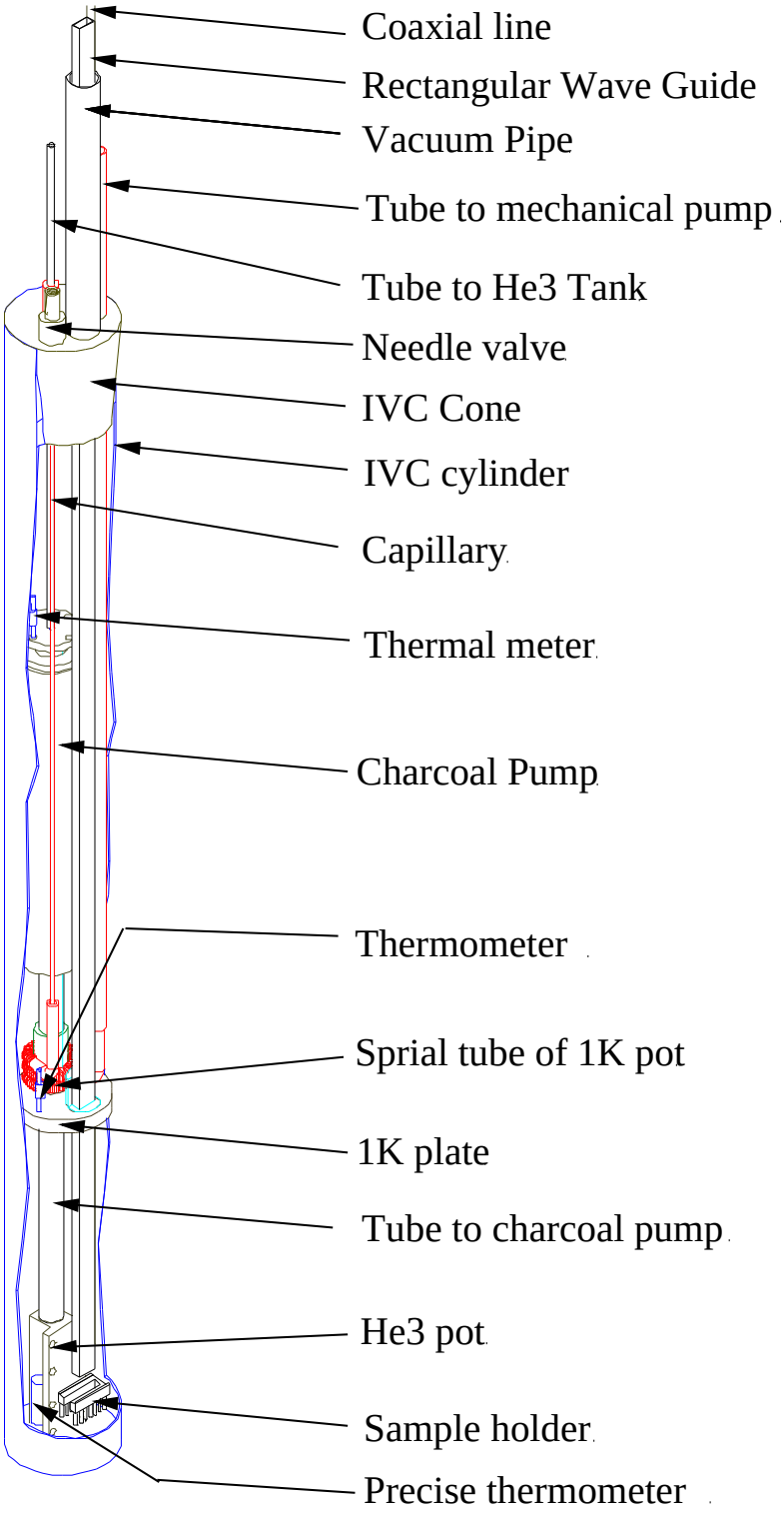

Fig. 2.1: The IVC dipped in liquid ^4He.

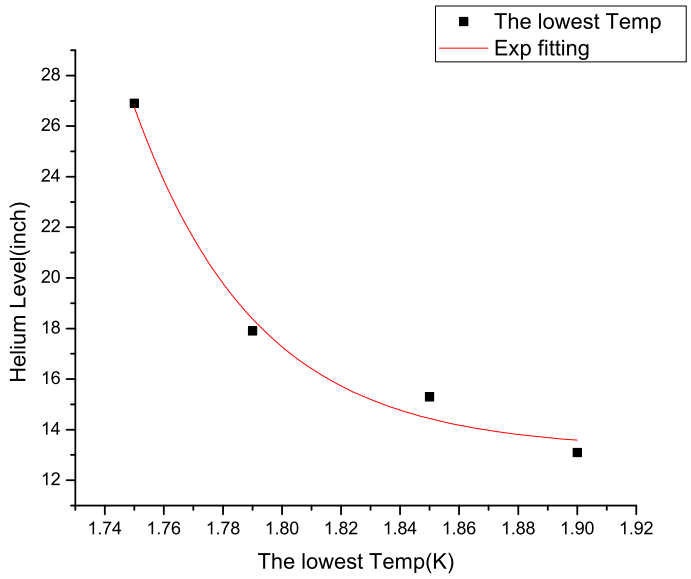

Fig. 2.2: The relation between ^4He level and the lowest temperature of the 1K-plate. At higher ^4He level, the heat load of 1K-plate is lower.

down the 1K-plate to about 2K. A needle valve regulates the flow providing the lowest possible temperature.

The temperature of the 1K-plate is determined by different factors such as the pumping rate, setting of the needle valve and the level of the^4He bath and thermal loads on the 1K pot. ^4He is pumped away from the other end of the copper tube. A strong pump improves the cooling power of the 1K pot. In our system, the lowest temperature of the 1K-plate has also a correlation with the level of ^4He liquid surrounding the insert. This is shown in Fig. 2.2

When the temperature of the 1K-plate is below 2.5 K, the ^3He gas condenses into the He^3 pot. During the condensation process the heater of the charcoal pump is switched

on. So that the gas absorbed by the sorption pump is driven out and is condensed by the 1K-plate. Condensation of $5cm^3$ of the liquid ^3He takes 20-25 minutes. After the condensation, the heater is switched off and the pump starts to absorb the ^3He gas. The pumping reduces the vapor pressure of the ^3He gas and lowers the temperature of the liquid ^3He. The lowest temperature, T=0.27K, is reached usually after 25 min of pumping. The ^3He system can maintain this temperature for 24 hours. The sorption pump is an important part of the system. The pump uses porous charcoal to absorb ^3He gas. The active charcoal is able to absorb high volumes of gas. In our device, 22g of the active charcoal can handle a full pot of ^3He liquid (about 5 cm^3 of liquid He^3). Temperature sensors provide us very important information about the performance of the refrigerator. One commercial calibrated Ruthenium Oxide thermometer (LakeShore) is placed on the ^3He pot. Other two temperature sensors are made from carbon resistors and are calibrated by the Ruthenium Oxide thermometer. The thermometers are placed on the ^3He pot, on the 1K-plate and on the charcoal pump as shown in Figure 2.1. The thermometers are weakly dependent on magnetic field. A computer aid design (CAD) software has been used for the design of the ^3He refrigerator. One of the advantages of the CAD is virtual assembling, which greatly facilitates the design process.

2.2 Super Conducting Magnet

In our main cryostat, a custom designed 90 kilogauss magnet at 4.2K is installed. The super conducting magnet was built using twisted multi filamentary NbTi wire in a copper matrix. The coil is completely epoxy impregnated to prevent training . The copper matrix in the wire acts as a form of quench protection along with diodes. These magnet has been designed for +/- 0.1% homogeneity over 1 cm diameter spherical volumes with helium level sensor.

Persistent Mode

Our magnet is equipped with a Persistent Switch, which is a piece of superconducting wire with heater shorts its input power terminals. Superconducting magnets have one particularly nice capability over resistive magnets. Once a current has been placed inside the magnets, virtually no power is need to maintain that current. When the magnet is being charged, the persistent switch heater is turned on so the short across the magnet terminals is driven above its critical temperature and effectively becomes a resistor across the magnet terminals. When the appropriate operating current in the magnetic is reached, the heater can be shut off and the persistent switch cools down until it becomes superconducting. At this point the power source to the magnet is no longer needed.

2.3 Microwave Transmission

In our experiments, the high frequency AC signals such as microwaves signals are used. Microwaves are electromagnetic waves with wavelengths which extend over a range of 1m-0.1mm and 300 Mhz-3000Ghz in frequency. To transmit microwave energy, a coaxial line and waveguide have been used in our experiments. The coaxial lines transmit microwaves up to 20 GHz. A rectangular stainless steel waveguide is used at higher frequencies from 20 to 40 GHz.

The Microwave Transmission Design at Low Temperatures

In our ^3He cryostat there are two microwave channels, a waveguide and a coaxial line. We used a stainless steel waveguide and coaxial line to strongly reduce the heat link between the IVC and room temperature because of the low heat conductivity of the stainless steel. The transmission lines are anchored at the IVC cone and the 1K-plate. This design facilitates cooling of the transmission lines and minimizes the heat load of the ^3He pot, because the IVC cone spends cooling power from the liquid Helium bath instead of the refrigerator. To prevent room temperature radiation through the hollow waveguide, an infrared filter made of a Gore-Tex material is inserted into the waveguide. The filter absorbs effectively the infrared radiation above 40K.

In order to keep the vacuum inside the IVC, a vacuum seal is required when microwaves are introduced. But the rectangular shape waveguide cracks easily at low

temperatures due to thermal expansion. Thus the whole vacuum seal could be destroyed, although the transmission of microwave is still available. Our solution is using a round stainless steel tube as a waveguide closure. On top of the waveguide, a plug made with Pyrex glass is used to seal the waveguide from the outside but is transparent to microwave signals.

2.4 Data Acquisition Hardware

The electronic measurement system contains several parts: AC Lock-In Amplifiers, driving current circuits and a four-points probe measurement circuit. In the four probe scheme, a current is applied between a source and drain of the sample and potential difference (voltage) is measured between two potential contacts of the sample area. The setup is depicted in Fig. 2.3. An external AC output of the Lock-In amplifier (Stanford Research System model SR-830) provides a low frequency AC voltage applied to a resistor, which is in series with the sample. The resistance of the resistor is significantly higher than the sample resistance R_s, providing a current, which is nearly independent on R_s. Usually, we used 10MΩ or 400MΩ resistors. The strength of the driving current is chosen to be small enough to prevent possible overheating of the samples at low temperatures. We used an AC excitation to avoid possible parasitic thermoelectric effects and to increase the signal to noise ratio. Because of a finite capacitance of electrical line, an out-phase signal appears in the measurements, the measurement frequency is selected to minimize the out-phase signal.

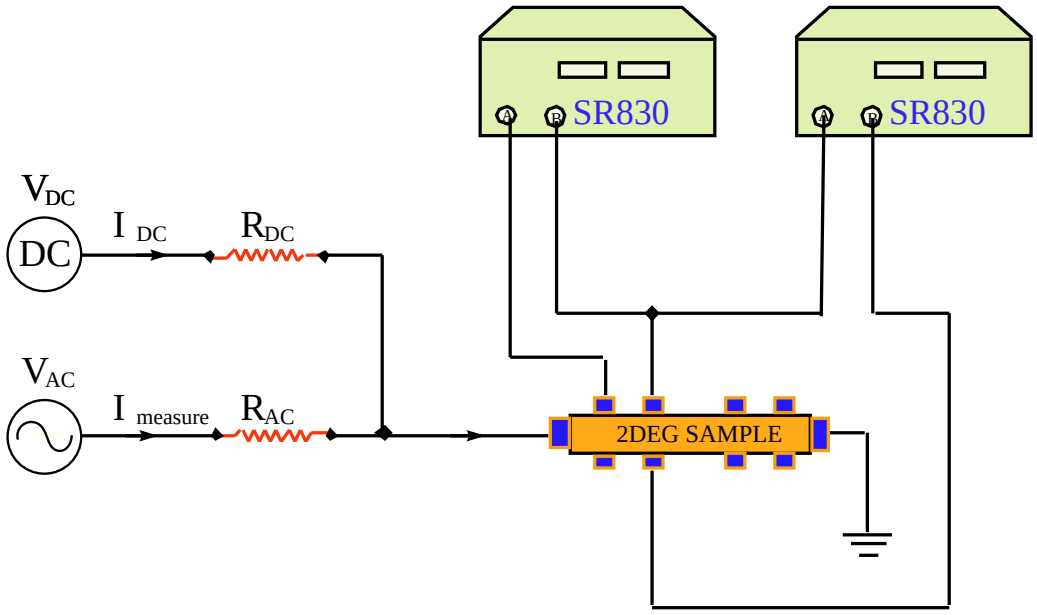

Fig. 2.3: The electrical connection of measurement in experiments

Other subsystems control the experimental parameters: magnetic field, microwave power, temperature, and others. The magnetic field is controlled by a power supply (CS-4, Cryomagnetics) which provides a current to superconducting magnets. The four-quadrant supply generates a continuous and smooth sweep of the magnetic field from -9T to +9T. An automatically stabilized microwave generator (Anritsu 68369A/NV) provides a calibrated AC signal from 100Mhz to 40Ghz with a 1Hz resolution. The temperature control of the experimental setup is more complex. The most important part to measure and control is the ^3He pot. The temperature of the ^3He pot is controlled by a PID controller (SIM 9600, Stanford Research), using an AC bridge (SIM 921, Stanford Research) to measure the temperature of the ^3He pot. The system provides 3% temperature stabilization in the interval 0.3K to 2K. For

higher temperatures an independent PID controller (bridge/controller model 1000 of BTI, INC) also controls the temperature of the sorption pump. The temperatures of other parts of the ^3He insert are monitored by Agilent 34401A multimeters.

2.5 Data Acquisition Software

The data acquisition software is written in Labview language. Most instruments are controlled through a GPIB interface. The software provides automatic measurements with high precision. The block diagram of the software is shown in Fig. 2.5.

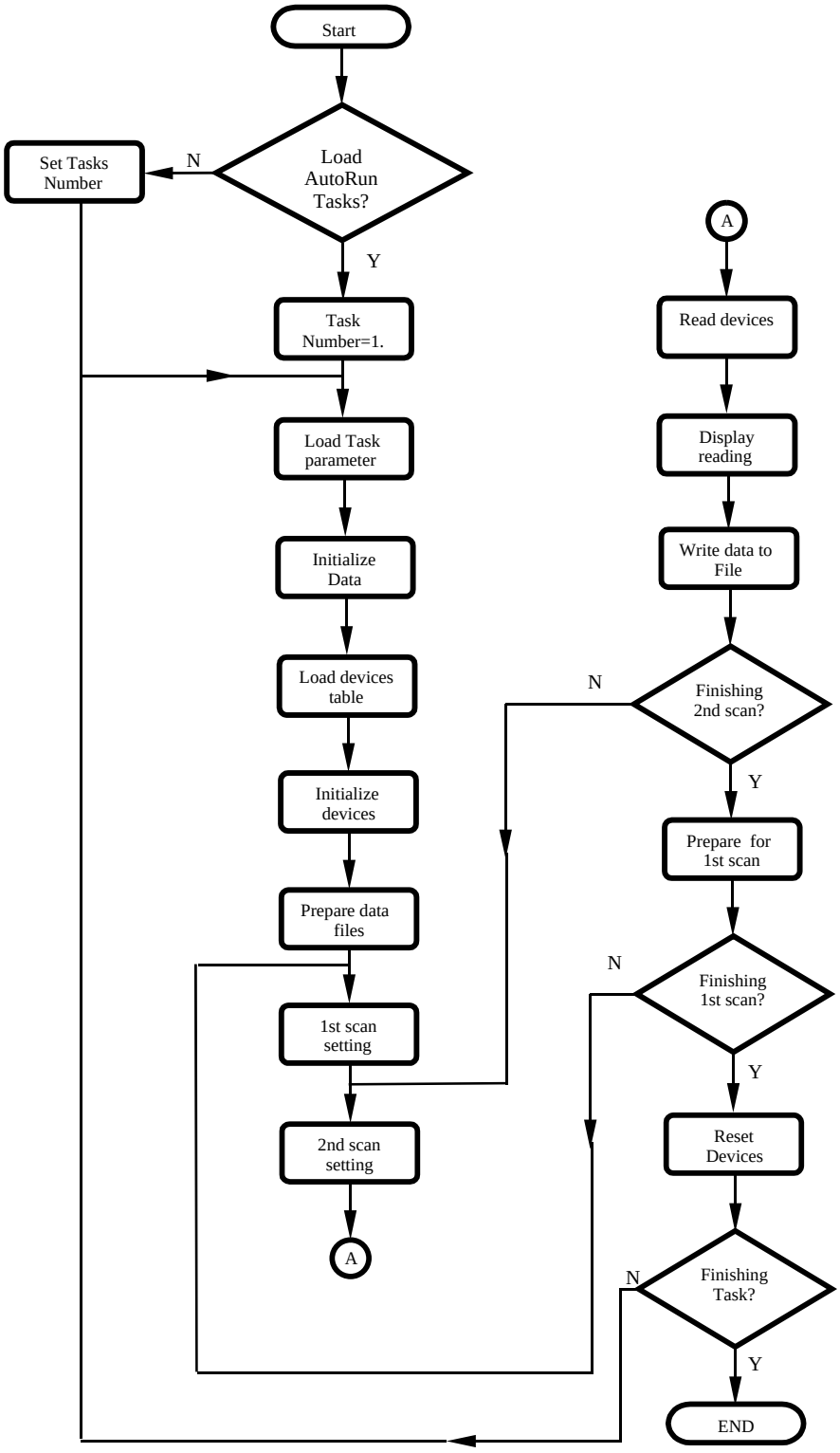

Fig. 2.4: Flow chart of the data acquisition software

3. EFFECT OF DC AND AC EXCITATIONS ON THE LONGITUDINAL RESISTANCE OF A TWO-DIMENSIONAL ELECTRON GAS IN HIGHLY DOPED GAAS QUANTUM WELLS

3.1 Introduction

Nonlinear properties of highly mobile two dimensional electrons in AlGaAs/GaAs heterojunctions is subject of considerable current interest. Several new transport phenomena have been observed in these systems recently [6, 8, 5]. In the pioneer work [6] a strong oscillations of the longitudinal resistance induced by microwave radiation have been observed at magnetic fields, which satisfy the condition $\omega = n \times \omega_c$, where ω is the microwave frequency and ω_c is cyclotron frequency. At higher level of the microwave excitations minimums of the oscillations can reach very low values, which are close to zero [8, 14, 13]. This so-called zero resistance state (ZRS), initiated extensive interest to the problem. Several theoretical approaches have been proposed to explain the strong oscillations of the conductivity as well as the ZRS [10, 15, 16, 17, 18].

Another interesting nonlinear phenomenon has been observed in the response of the 2D highly mobile electrons to DC excitations [5]. Oscillations of the longitudinal

resistance, which are periodic in inverse magnetic field, have been found at DC biases, satisfying the condition $\hbar\omega_c = 2R_cE_H$, where R_c is Larmor radius of electrons at Fermi level and E_H is Hall electric field, induced by the DC bias in the magnetic field. The effect has been attributed to Zener tunneling between Landau orbits, tilted by the Hall electric field [5]. This was discussed in the chapter of introduction in more detail. In this section we discuss our observations of the nonlinear resistance oscillations with magnetic field in DC biased GaAs quantum well with 2D electron density of an order of magnitude higher than the one reported earlier. This is, probably, the first independent confirmation of the results obtained by the group of prof. Du [5]. Moreover we have found similar resistance oscillations with magnetic field in response to low frequency (10 KHz and 100 KHz) and high frequency (1 MHz to 20 GHz) AC excitations. The particular form of the resistance oscillations at the AC excitations is considerably different from the DC case. We show experimentally that for the low frequencies (10 KHz, 100 KHz) the difference is the result of an average of the DC differential resistance during a period of AC excitations. Although at high frequencies we were not able to measure unambiguously the magnitude of the AC current through the sample, we suggested, that a similar average could be applied for the oscillations of 2D resistance, induced by RF and microwave excitations.

3.2 Experiment

Our samples were cleaved from a wafer of a high-mobility GaAs quantum well grown by solid source molecular beam epitaxy on semi-insulating (001) GaAs substrates. The width of the GaAs quantum well was 13 nm. AlAs/GaAs type-II superlattices served as barriers, which made it possible to obtain a high-mobility 2D electron gas with high electron density [19]. Without light illumination, the electron density and mobility of the 2D electron gas in our samples were $n_e = 1.18 \times 10^{16}$ m^{-2} and μ= 91 m^2/Vs, respectively. After brief light illumination, the electron density and mobility of the 2D electron gas in our samples were $n_e = 1.28 \times 10^{16}$ m^{-2} and μ= 111 m^2/Vs, respectively. Measurements were carried out at T=4.2 K in magnetic field up to 1 T on 50 μm wide Hall bars with distance of 250 μm between potential contacts. Microwave radiation was supplied to the sample through a coaxial cable and was fed to the 2D electron gas through current contacts of the Hall bars. The longitudinal resistance was measured using 1 μA current at frequency of 888 Hz. Three samples are measured. All samples demonstrate the same behavior.

3.3 Results

Dependence of the longitudinal resistance r_{xx} of the 2D electron gas is presented in Fig. 3.1 at different values of the DC bias. A positive magnetoresistance of the sample is observed at zero DC bias. At a finite DC bias a strong negative magnetoresistance

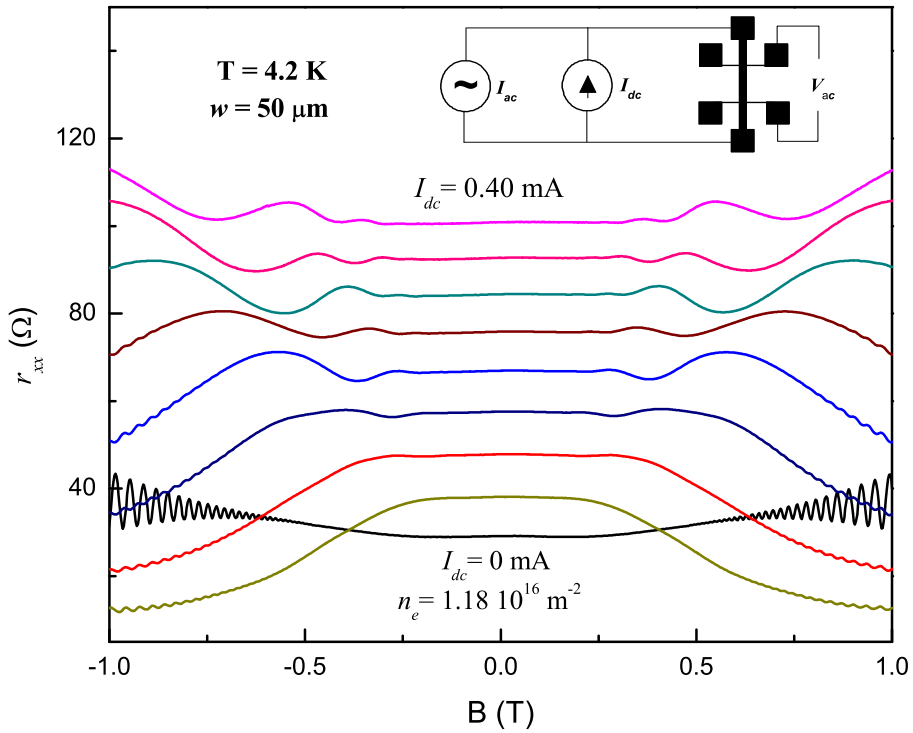

Fig. 3.1: Dependence of the differential resistance r_{xx} on magnetic field at different DC current from 0 mA to 0.4 mA in steps of 0.05 mA. For clarity, the curves are shifted vertically by $n\times 8$ Ohm, where n=0,1...8. The experimental setup is shown on the top.

occurs. With an increase of the DC current through the sample, non-monotonic, oscillating behavior of the longitudinal resistance is found, similar to reported earlier [5]. The positions of maximums (minimums) of the oscillations depend on the DC bias. To make a direct comparison with previous measurements, we obtain numerically the first derivative of the curves with respect to magnetic field. The result is presented in Fig. 3.2a. Apparent oscillations of the dr_{xx}/dB are periodic in the inverse magnetic

field. It is shown in the inset to Fig. 3.2a. The positions of the oscillation maximums B_l in magnetic field correspond to the condition: $l \times \hbar\omega_c = \gamma R_c \times eE_H$, where $\gamma \approx 2$ [5]. At this condition "horizontal" transitions between tilted Landau levels are possible with a momentum transfer $\Delta k_x \approx 2k_F$, where k_F is the electron wave vector at Fermi level.

The positions of the maximums of the dr_{xx}/dB are proportional to current density (see Fig. 3.2b). From slopes of the linear dependencies of the dr_{xx}/dB maximums on the DC density we have found γ= 2.06; 2.13; and 2.18 for l=1,2, and 3 correspondingly. These values are close to the ones obtained in the previous work[5].

As we mentioned above, the main experimental and theoretical efforts have been applied toward understanding the microwave induced oscillations of the resistance and the ZRS in the 2D electron gas [6, 8, 13, 14]. The observed oscillations occurs at microwave frequency ω, which is close to a multiple of the cyclotron frequency $n \times \omega_c$: $\omega \approx n \times \omega_c$, where $n = 1, 2...$ is an integer. The oscillations exist in the so-called cyclotron resonance regime, at which the frequency of microwave radiation is much higher than the momentum relaxation rate $1/\tau_p$: $\omega \gg 1/\tau_p$, where τ_p is transport the mean free time. The low frequency excitation regime: $\omega\tau_p < 1$ has not been explored yet. However, as shown above, even in the pure DC case there is very rich nonlinear physics. Below we present the study of magneto-oscillations of the 2D longitudinal resistance induced by AC external excitations observed in a broad frequency range corresponding to the condition $\omega\tau_p < 1$.

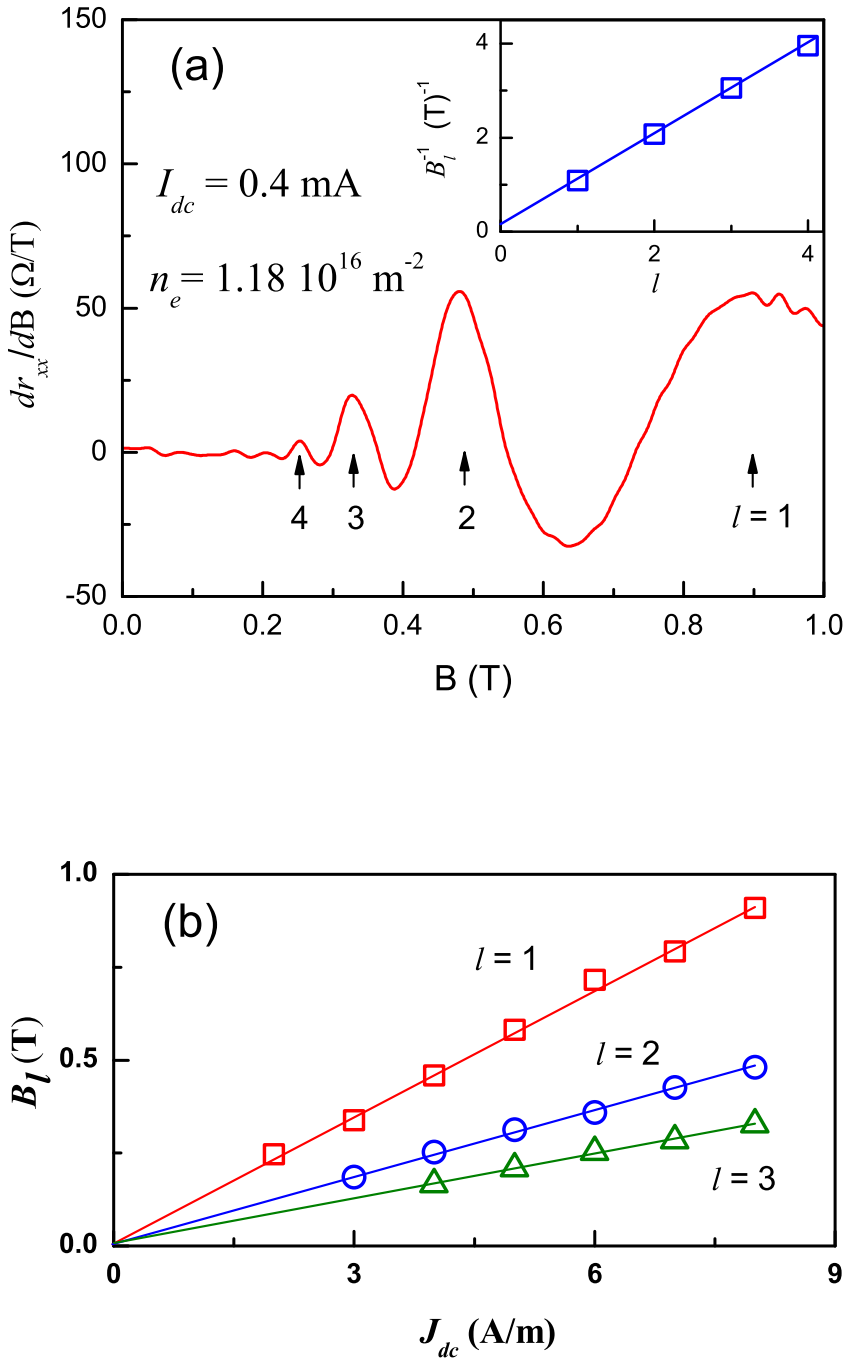

Fig. 3.2: (a) Dependence of the derivative dr_{xx}/dB on magnetic field at $I_{dc} = 0.4$ mA The inset demonstrates the $1/B$ periodicity extracted from the dr_{xx}/dB trace. (b) Positions of oscillation maximums $B_l (l = 1, 2, 3)$ versus DC current density J_{dc}. A linear fit reveals the relation $B_l \propto J_{dc}/l$.

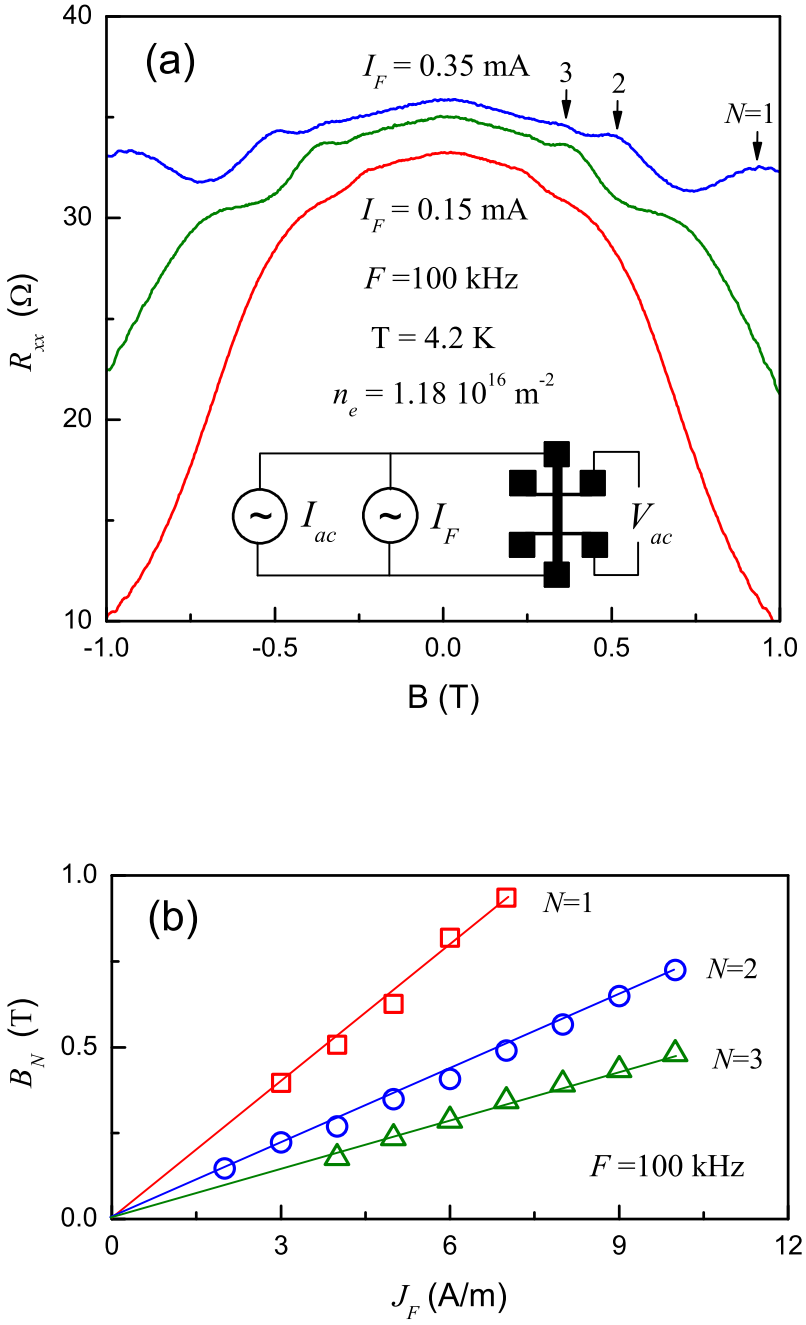

Fig. 3.3: (a) Magnetoresistance R_{xx} at different amplitudes of AC excitation. Maximums of the resistance oscillations are marked by arrows. Positions of the maximums are approximately periodic in $1/B$. A diagram for the electrical measurement is presented at the bottom of the figure. (b) The oscillation maximums B_N ($N = 1, 2, 3$) versus current density J_F. Linear fit reveals the relation $B_N \propto J_F/N$.

A dependence of the longitudinal (888 Hz) resistance on magnetic field at different level of AC excitation (100 kHz) is presented in Fig. 3.3a. The figure demonstrates oscillations of the linear resistance with magnetic field. Positions of the resistance maximums B_N indicated by arrows in Fig. 3.3a are plotted as function of the magnitude of the 100 kHz excitation current in Fig. 3.3b. The position of the maximums are proportional to the magnitude of the AC density J_F. The maximum positions are periodic in the inverse magnetic field.

Similar oscillations of the linear resistance with magnetic field are found at different level of RF and microwave excitations in the frequency range from 1MHz to 20 GHz. One of the dependencies is presented in Fig. 3.4a at excitation frequency 11 GHz. The oscillations are found to be periodic in the inverse magnetic field. The periodicity is shown in Fig. 3.4b. Positions of the oscillation maximums depend on the microwave power: maximums move to higher magnetic fields at higher level of the microwave power P_ω. For a linear microwave circuit current density through the sample should be proportional to square root of the input microwave power $J_\omega \sim (P_\omega)^{1/2}$. We have found that the positions of the maximums in the magnetic field is not proportional to the $(P_\omega)^{1/2}$ (see Fig. 3.4c). We suggest that due to strong dependence of the sample resistance on the external microwave radiation the actual magnitude of the microwave current applied to the sample does not follow the square root rule. Additional microwave experiments are required to check the dependence of the maximums on the applied microwave current.

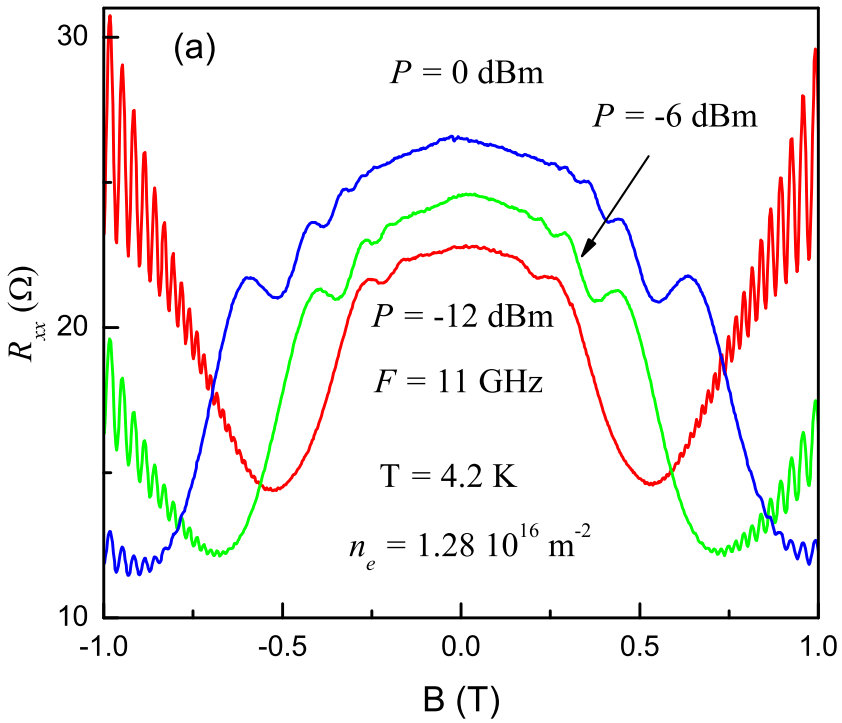
(a)
P = 0 dBm
P = -6 dBm
P = -12 dBm
F = 11 GHz
T = 4.2 K
n_e = 1.28 10^16 m^-2
R_xx (Ω)
B (T)
30
20
10
-1.0
-0.5
0.0
0.5
1.0

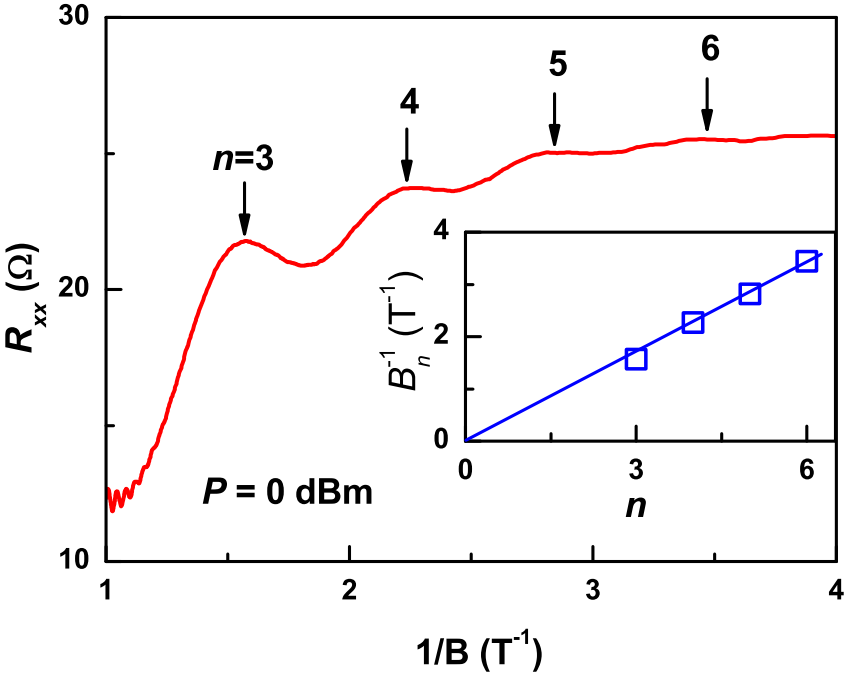
n=3
4
5
6
P = 0 dBm
R_xx (Ω)
1/B (T^-1)
B_n^-1 (T^-1)
n
30
20
10
1
2
3
4
0
2
4
0
3
6

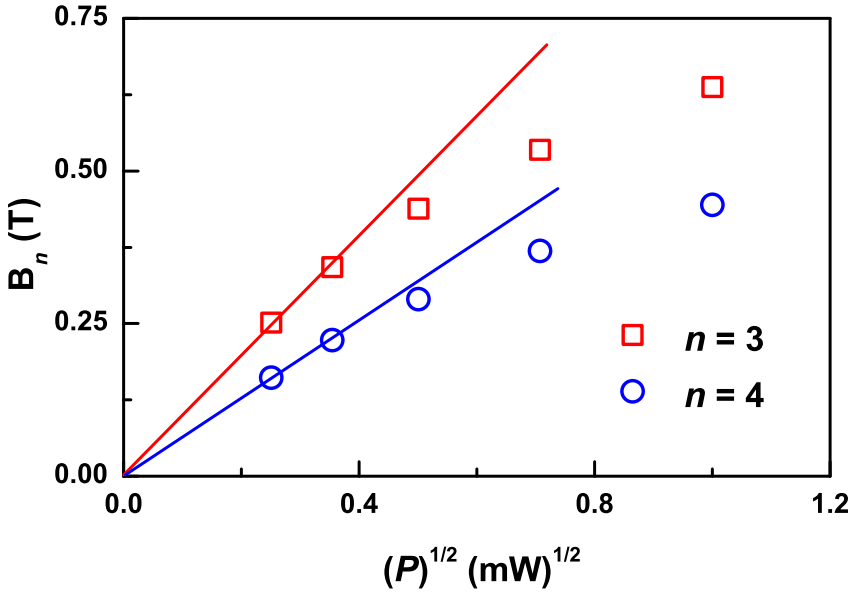

Fig. 3.4: (a) Magnetoresistance R_{xx} at different levels of microwave power as labeled. (b) Dependence of the longitudinal resistance on inverse magnetic field $1/B$ at microwave excitation $P = 0$ dBm. Insert demonstrates the $1/B$ periodicity of the oscillations. (c) Position of the oscillation maximums vs square root of input microwave power. Figures (b) and (c) are obtained at the same conditions as Fig. 3.3a.

Below we present the response to the low frequency (10 KHz , 100KHz) excitations with well controlled current amplitude (see Fig. 3.3). We will show that oscillations of the resistance at frequency 888 Hz with magnetic field are a result of a special average of DC I-V curves. In other words the AC non-linear response at frequency below 100 kHz is a direct consequence of the non-linearity at zero frequency.

The low frequency experimental setup is shown in Fig. 3.3a. The testing current I_{ac} at frequency 888 Hz and AC excitation current I_F at frequency $F = 10/100$ kHz are applied through current leads of the sample, using twisted pairs of conducting wires. Due to negligible effect of the current leakage through a capacitance between the wires at used frequencies, the AC currents were fixed with accuracy better than 5% during measurements. The AC voltage V_{ac} at frequency 888 Hz were measured using standard lockin amplifier synchronized with the testing current I_{ac}.

3.4 Discussion

Since at frequency 888 Hz the response is linear with respect to the testing current I_{ac} we approximated the response by Ohm's law :

$$V_{ac} = R_{xx}(I_F) \times I_{ac} \tag{3.1}$$

where $R_{xx}(I_F)$ is a resistance of the sample, which depends on the external AC current $I_F = I_0 cos(2\pi F t)$, where I_0 is amplitude of the AC excitation. One can expand the

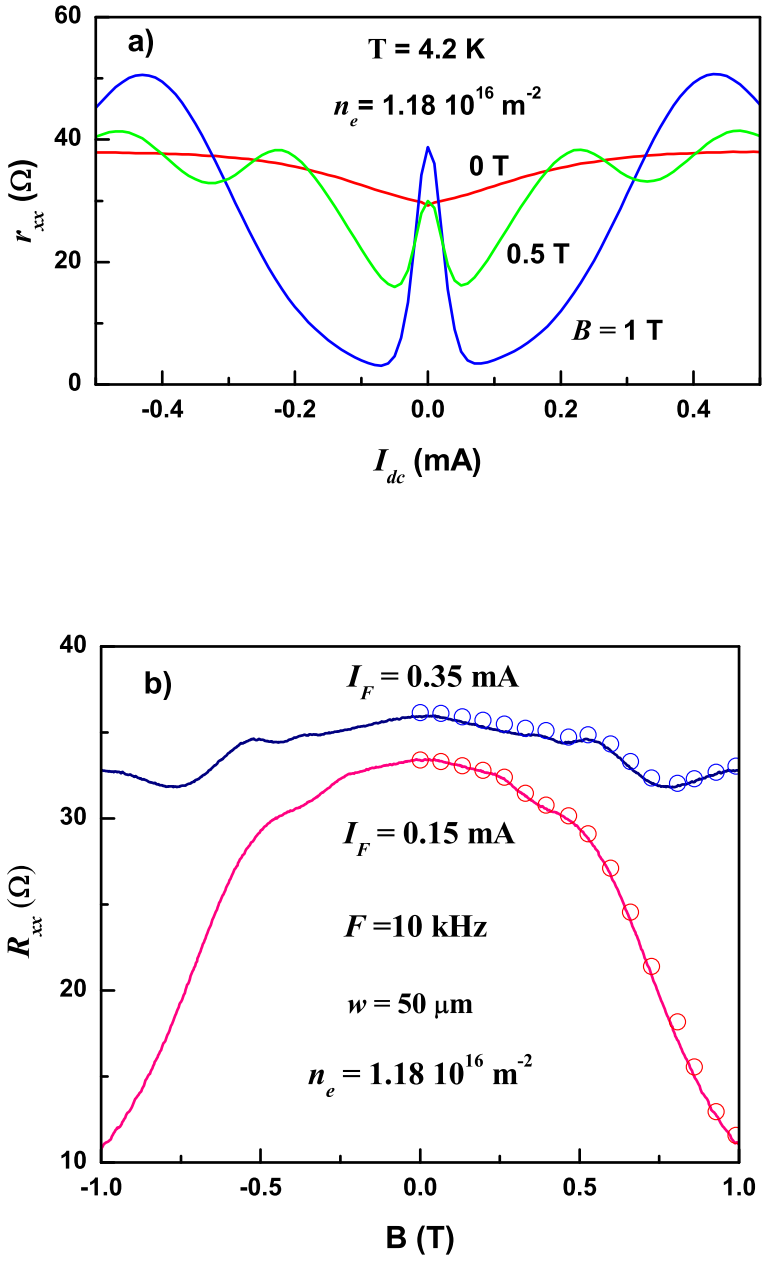

Fig. 3.5: (a) Dependence of differential resistance r_{xx} on DC bias at different magnetic field B as labeled. (b) Measured magnetoresistance R_{xx} at two different levels of AC excitations as labeled (solid lines). Calculated magnetoresistance obtained from the DC biased measurements in Fig. 3.5a (open dots). The procedure is described in text. No adjusting parameters are used for the comparison.

resistance $R_{xx}(I_F)$ in a sum of all possible harmonics ($i \times F$) of the external AC current:

$$R_{xx}(I_F) = \Sigma R_i(I_0) \times cos(i \times 2\pi F t) \tag{3.2}$$

where $R_i(I_0)$ a Fourier component of the $R_{xx}(I_F)$ at a frequency $i \times F$ and $i = 0, 1, 2...$ is an integer.

The lock-in amplifier locked at frequency 888 Hz measures exclusively the zero frequency (i=0)harmonic R_0, because only the R_0 provides a term oscillating at frequency 888 Hz in the Eq. (3.1). Thus to find the resistance $R_{xx}(H)$ at a magnetic field H one has to obtain the zero frequency harmonic of the $R_{xx}(I_0, H)$:

$$R_0(H) = 1/T \int R_{xx}(I_0 cos(2\pi F t) dt \tag{3.3}$$

where $T = 1/F$ is a period of the AC excitation.

In order to perform the integration in the Eq. (3.3), we need to know the dependence of the resistance R_{xx} on the driving current I. This is done at zero frequency (DC case). The dependence of R_{xx} on the current I_{dc} (in fact the differential resistance r_{xx} (see Fig. 3.1) was measured at different magnetic fields. The dependence is presented in Fig. 3.5a at several magnetic fields as labeled. Using the experimental data, the integration in Eq. (3.3) was performed numerically. Values of the average resistance R_0 were obtained for different magnetic fields. Calculated resistance R_{xx} is presented

in Fig. 3.5

Measured dependencies of the resistance $R_{xx}(H)$ on magnetic field at two different amplitudes of the external AC excitations are also shown in the figure for a comparison (solid lines). We note, that there are no adjusting parameters between measured and calculated curves. Similar results are obtained at 100 KHz frequency (not shown). The agreement indicates the validity of the interpretation of the AC induced oscillations of the longitudinal conductivity based on the special average of the differential resistance r_{xx}.

4. NONLINEARITY OF THE LONGITUDINAL RESISTANCE OF TWO-DIMENSIONAL ELECTRONS IN A MAGNETIC FIELD INDUCED BY A SMALL DC ELECTRIC FIELD

4.1 Introduction

In the previous chapter, the strong nonlinearity of 2D magnetoresistance induced by a *dc* electric field was shown. In this section we will present experiments, which identify the dominant mechanism responsible for the nonlinear response of the 2D electron systems at a small electric field E (at small *dc* bias). Historically the experiments have been performed to study the unusually strong reduction of the resistance r_{xx} at small *dc* bias, which has been observed in our experiments [20] presented in the previous chapter (see Fig. 3.5a). This strong drop in the resistance with the dc bias at a fixed magnetic field has not been clearly identified in the original paper [5], because the authors were focused on the magnetoresistance oscillations at a fixed *dc* bias.

The intriguing point is that the strong reduction of 2D longitudinal magnetoresistance occurs at small *dc* electric fields E_H, which are substantially smaller than the ones required for the "horizontal" (Landau-Zener) transitions between Landau levels[5, 20]. This may indicate a new mechanism of nonlinearity dominating at small *dc* biases.

Moreover, in contrast to the inter-Landau level scattering, we have found the effect at small *dc* bias to be strongly dependent on the temperature. This main experimental finding allowed us to identify later on the physical origin of the nonlinearity.

After critical analysis of an extended amount of different theoretical models (overwhelming majority of them advocating for the Landau-Zener type mechanism), we have found one, which describes reasonably well our results[10]. Following the theory we suggest that the strong reduction of the resistivity in our experiments is due to a substantial and nontrivial deviation of the electron distribution function from equilibrium condition induced by the electric field E_H. The deviation is result of a non-uniform spectral diffusion electrons through the Landau levels. We are very pleased that our paper [22] has been recognized as one of the three significant publications in condensed matter physics in September 2006 by Journal Club for Condensed Matter Physics [23].

4.2 Samples and Experiment

The experiments are done on the samples, which were cleaved from a wafer of high-mobility GaAs quantum well grown by molecular beam epitaxy on semi-insulating (001) GaAs substrates. The width of the GaAs quantum well was 13 nm. AlAs/GaAs type-II superlattices served as a barriers, which made possible to obtain a high-mobility 2D electron gas with high electron density [19]. We have studied two samples. The electron density and mobility of the 2D electron gas in the samples were $n_1 =$

1.22×10^{16} m^{-2}, $n_2 = 0.84 \times 10^{16}$ m^{-2},and μ_1= 93 m^2/Vs, μ_2= 68 m^2/Vs respectively at T=2.7K. In fact the samples are very similar to one we have use in our previous experiments[20].

Measurements were carried out between T=1.8 K and T=77 K in magnetic field up to 3.2 T on d=50 μm wide Hall bars with a distance of 250 μm between potential contacts. The longitudinal resistance was measured using a current of 0.5 μA at a frequency of 77 Hz in the linear regime. Direct electric current (bias) was applied simultaneously with AC excitation through the same current leads (see inset to Fig. 4.1). Although we have studied, strictly speaking, the differential resistance, for the sake of simplicity we will refer to it below as resistance.

4.3 Results and Discussion

Typical curves of the longitudinal resistance r_{xx} are shown as a function of the DC bias in Fig. 4.1 at two temperatures. At high DC bias the resistance exhibits maximums that satisfy the condition $n \times \hbar\omega_c = 2R_cE_H$, corresponding to "horizontal" transitions between Landau levels.[5, 20] Another striking feature is the sharp peak at zero DC bias which broadens as the temperature is raised. This zero bias peak is the main topic of this chapter.

The evolution of the magnetoresistance with DC bias and magnetic field is shown in Fig. 4.2. The zero bias peak appears at relatively high magnetic field $B \approx 0.2 - 0.3$ T (see Fig. 4.2a). At these fields the Landau level width $\hbar/\tau_q$ extracted from the

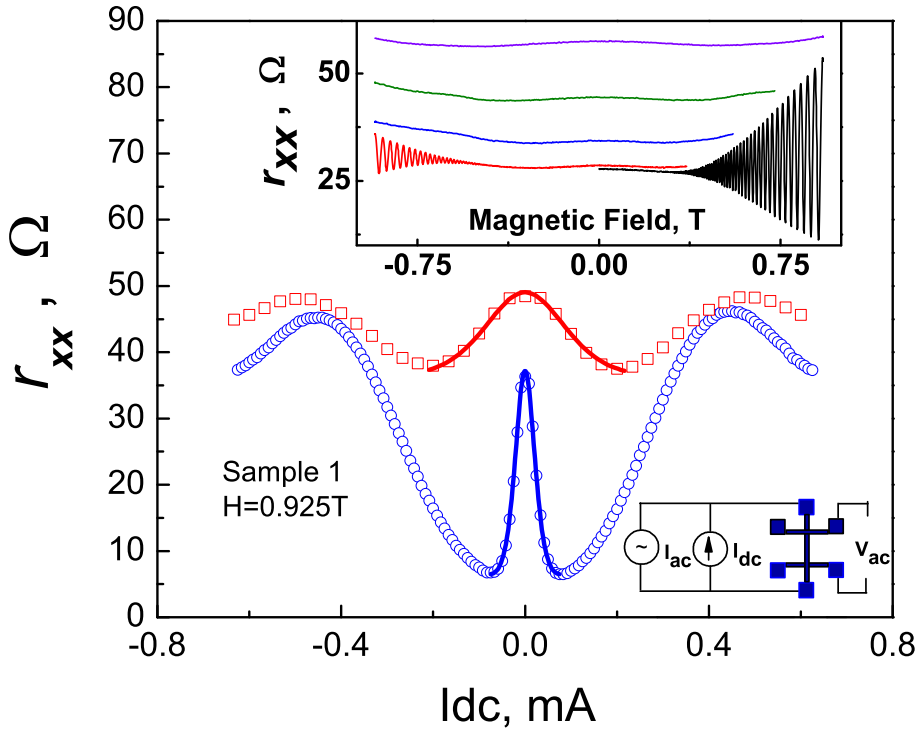

Fig. 4.1: (Color online) Dependence of the differential resistance r_{xx} on DC bias at B=0.925T. Circles correspond to T=4.3 K, squares correspond to T=19.8 K. The solid lines are theoretical curves obtained from Eq. 3. The fitting parameters are I_0=0.055 mA and δ=0.334 for T=4.3K and I_0=0.1802 mA and δ=0.177 for T=19.8 K. The top inset shows quantum oscillations of the longitudinal resistance at different temperatures T=1.9 K (bottom curve, right), 4.2 K (bottom curve, left), 9.9, 19.8 and 35 K (remaining curves in ascending order);$I_{dc} = 0A$. The experimental set-up is shown at bottom right.

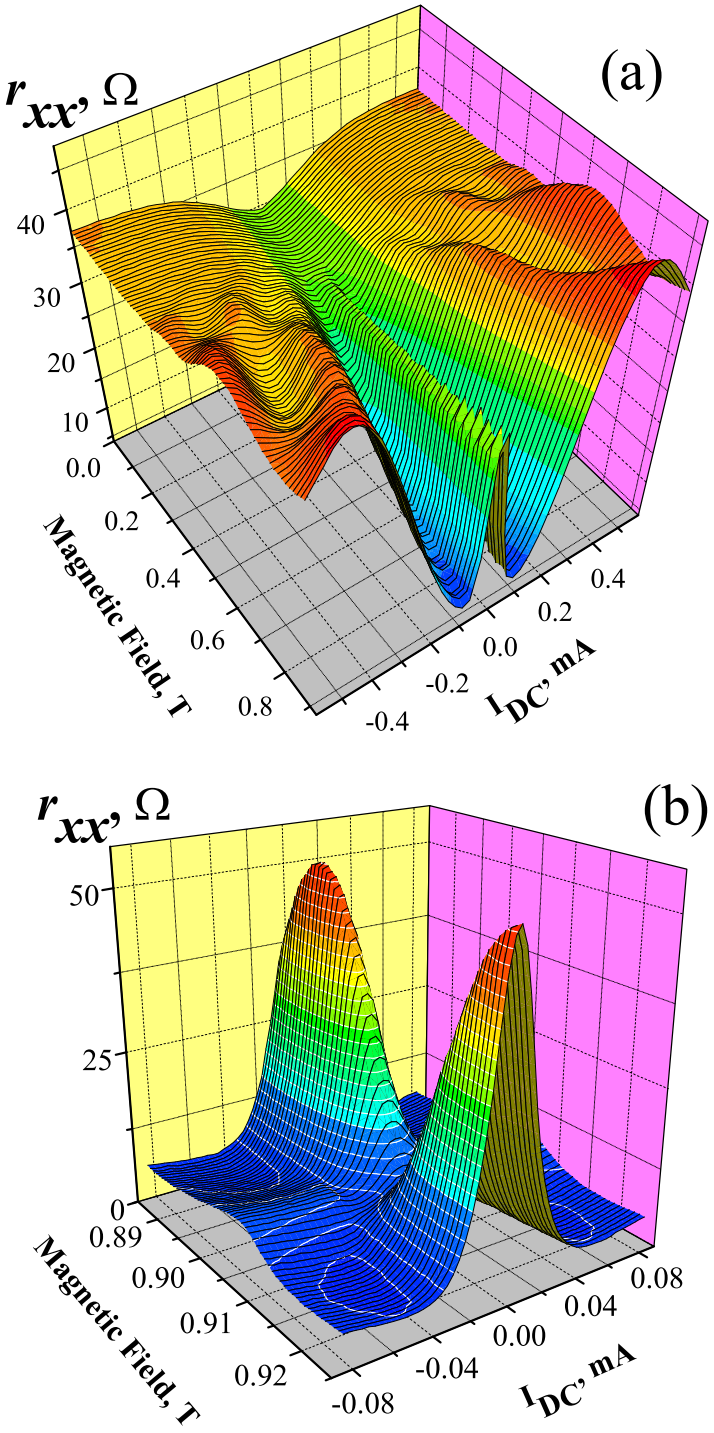

Fig. 4.2: (Color online) (a) The differential resistance r_{xx} as a function of magnetic field and DC bias at temperature T=4.3 K. (b) A similar plot at T=1.9 K over a narrower range of the experimental parameters, yielding better resolution.

amplitude of Shubnikov de Haas (SdH) oscillations becomes comparable with $\hbar\omega_c$, and the SdH oscillations are visible at low temperatures (see curve at T=1.9K in the top insert to Fig. 4.1). The strength of the peak increases gradually with magnetic field. Clear SdH oscillations are present in high magnetic field at zero bias. The magnitude of the SdH oscillations at T=4.3 K is substantially smaller than the amplitude of the zero bias peak. The peak is still present at temperatures above T=30K where no SdH oscillations are detected. A better resolved snapshot of the peak evolution is shown in Fig. 4.2b. The figure demonstrates the effect at low temperatures T=1.9K, where the SdH oscillations are well developed.

The striking reduction of the resistance is observed at high temperatures where no SdH oscillations are present. This is quite different from what one expects for electron heating by the electric field. As shown in the insert to Fig. 4.1, the resistance increases for higher temperatures, in contrast with the observed decrease with applied electric field. It should also be noted that at low temperatures, the largest effect possible due to heating is to reduce the resistance from its value at a SdH maximum to the "average" baseline value (which is ≈26-28 Ω in the insert to Fig. 4.1). The observed reduction in Fig. 4.2b is much greater than this, indicating this is a new phenomenon associated with the application of an electric field.

Below we compare our results with the theory.[10]. The theory is presented in chapter 1 in a general form. Here we recall briefly main parts, emphasizing details significant for the comparison. The theory considers 2D electrons in classically strong magnetic

field at finite electric field E_{dc} and at relatively high temperature $kT > \hbar\omega_c$. Due to conservation of total electron energy $(\epsilon + eE_{dc}x)$ in the DC electric field E_{dc}, the spatial electron diffusion translates into the diffusion of the electrons in energy space. The solution of the diffusion equation in ϵ-space yields nontrivial oscillations of the non equilibrium electron distribution function with period $\hbar\omega_c$. The temporal growth of the oscillations due to the diffusion is limited by inelastic electron-electron scattering, which smear the non-equilibrium contribution. The inelastic scattering time τ_{in} is inversely proportional to the square of the temperature (see section VII of ref. [10]) $\tau_{in} \sim 1/T^2$, making the stationary amplitude of the oscillations (and nonlinear conductivity) to be strongly temperature dependent. Relative to the Drude conductivity, σ_D, in zero magnetic field, the theory predicts a longitudinal conductivity[10]

$$\Delta\sigma_{xx}/\sigma_D = 2\delta^2[1 - \frac{4Q_{dc}}{1+Q_{dc}}], \tag{4.1}$$

where $\delta = exp(-\pi/\omega_c\tau_q)$ is the Dingle factor, τ_q is the quantum scattering time and the parameter Q_{dc} is

$$Q_{dc} = \frac{2\tau_{in}}{\tau_{tr}}(\frac{eE_{dc}v_F}{\omega_c})^2(\frac{\pi}{\hbar\omega_c})^2. \tag{4.2}$$

Here τ_{tr} is the transport scattering time and v_F is the Fermi velocity.

In order to compare with experiment, the differential conductivity at frequency ω, $\sigma_\omega = dJ/dE = d(\sigma(E)E)/dE$, is obtained using Eq.4.1. The variation of the differ-

ential resistance is found to be

$$\Delta r_{xx}/R_0 = 2\delta^2[\frac{1-10Q_{dc}-3Q_{dc}^2}{(1+Q_{dc})^2}], \tag{4.3}$$

where R_0 is the resistance at zero magnetic field. In a classically strong magnetic field $\omega_c\tau_{tr} \gg 1$, the DC electric field is almost perpendicular to the electric current I_{dc}: $E_{dc} = \rho_{xy}I_{dc}/d$, where d is the sample width. Using Eq. 4.2, we rewrite the parameter Q_{dc} in the form $Q_{dc} = (I_{dc}/I_0)^2$, where the scale I_0 is a fitting parameter. In accordance with Eq. 4.3, the parameter I_0 is directly related to the width of the zero bias peak and the peak magnitude is proportional to δ^2. Below we refer to the parameter I_0 as the line width. Examples of theoretical fits to the data using Eq. 4.3 are shown by the solid lines in Fig. 4.1, using δ and I_0 as fitting parameters.

The dependence of the width of the peak (I_0) on magnetic field is presented in Fig. 4.3 at different temperatures. At high temperature $kT > \hbar\omega_c$ ($\hbar\omega_c/k = 18K$ at B=0.925 T), the peak width varies considerably with magnetic field. The approximately linear increase of the scale I_0 with magnetic field agrees with the theory predicting the linear dependence (see Eq. 4.2 and $I_{dc} = E_{dc}d/(\rho_{xy} \sim$B)). The deviations from the linear dependence are beyond the scope of the theory. The oscillations could be related to magneto-phonon resonances observed in these systems at high temperature.[21] At low temperatures, $kT < \hbar\omega_c$, the width of the zero bias peak depends weakly on magnetic field, in contradiction with a simple extension of the high temperature

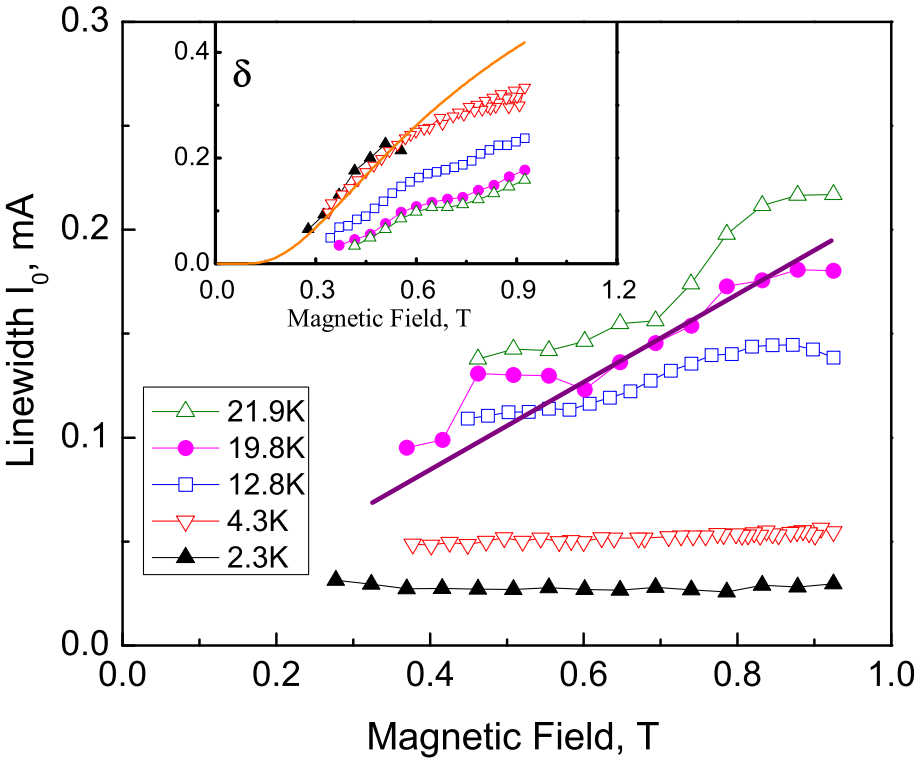

Fig. 4.3: (Color online) The dependence of the width of the peak I_0 on magnetic field at different temperatures, as labeled. The solid line represents the linear dependence expected from the theory in the high temperature limit (see Eq. 4.2). The inset shows the magnetic field dependence of the parameter δ obtained from the fit of the zero bias peak using Eq. 4.3. The solid line presents the theoretical dependence of the Dingle parameter δ on magnetic field, corresponding to a quantum scattering time τ_q=1.5 ps.

results (Eq. 4.1 and Eq. 4.2) to the low temperatures.

For several different temperatures, the insert to Fig. 4.3 shows the A dependence of the Dingle parameter, δ, which is obtained from comparison of the magnitude of the zero bias peak with the theory (see Eq. 4.3). The parameter δ decreases with decreasing magnetic field, and disappears below B=0.2T. We have plotted the parameter $\delta = exp(-\pi/\omega_c\tau_q)$, vs magnetic field using the quantum scattering time τ_q as a fitting parameter (see the solid line in the inset to the figure). The quantum time τ_q =1.5 ps obtained by the fitting is close to the quantum time extracted from the usual analysis of SdH oscillations at different temperature and/or magnetic field[4]. A comparison between these two results is shown in the bottom inset to Fig. 4.4. Using the new method, the quantum time τ_q is found for temperatures up to 24K, where SdH oscillations are absent and previous methods fail to work. Thus the method extends considerably the temperature range in which the quantum scattering time can be studied.

The temperature dependence of the width of the peak is shown in Fig. 4.4. At low temperatures the width of the peak is found to be proportional to the temperature T. At higher temperature a noticeable sublinear deviation is observed, followed by a super-linear temperature dependence of the line width at temperatures $T > 30$ K (not shown for sample N2). The solid lines in the figure are theoretical curves plotted in accordance with Eq. 4.2 in which the temperature variations of the transport time τ_{tr} (shown in the top inset to the figure) are taken into account. The inelastic

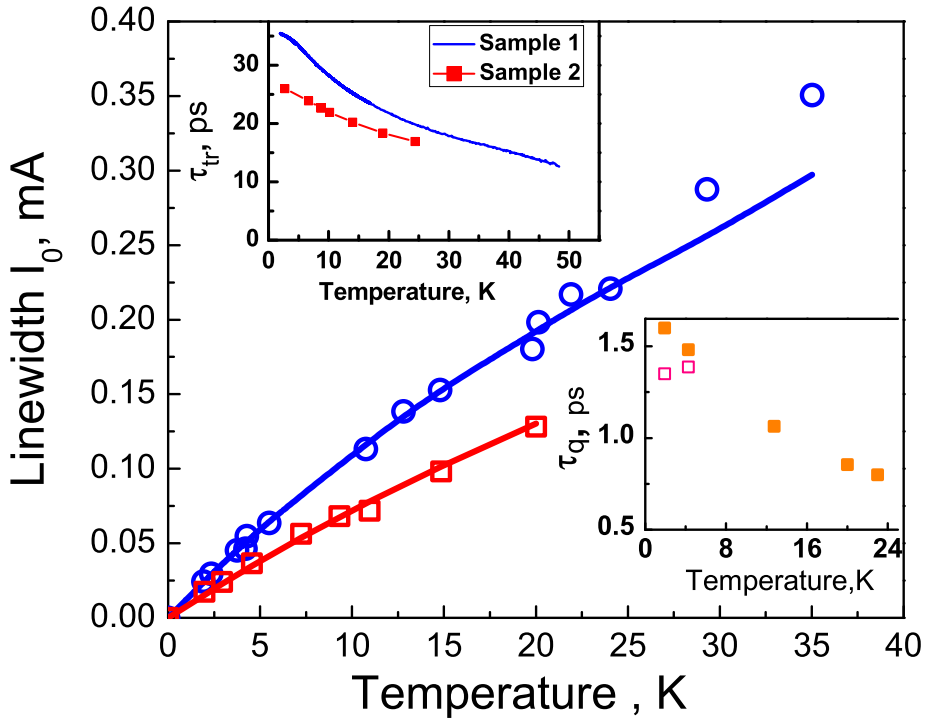

Fig. 4.4: (Color online) Dependence of the width of the zero bias peak I_0 on temperature for sample N1 (open circles) and sample N2 (open squares) at B=0.925T. The solid lines are the theory using Eqs. 2. The comparison gives an inelastic scattering time $\tau_{in} = 10/T^2(12/T^2)$ns for sample N1(N2). The top inset shows the transport time τ_{tr} vs temperature at zero magnetic field. The dependence of the quantum scattering time τ_q on temperature is shown in the bottom insert. Open squares correspond to τ_q determined from the amplitude of the SdH oscillations using Lifshits-Kosevich formula.[4] Filled squares are the τ_q determined by comparison of the amplitude of the zero bias peak with Eq. 4.3.

scattering time τ_{in} is approximated by the theoretical expression [10] $\tau_{in} = \alpha/T^2$ with the constant α used as the only fitting parameter. For the inelastic time we have found $\tau_{in}^{(1)} = 10 \times 10^{-9}/T^2$ s and $\tau_{in}^{(2)} = 12 \times 10^{-9}/T^2$ s for samples 1 and 2. The corresponding theoretical estimates[10] of the inelastic time give $\tau_{in,t}^{(1)} = 4.8 \times 10^{-9}/T^2$ s and $\tau_{in,t}^{(2)} = 3.2 \times 10^{-9}/T^2$ s. We consider this as satisfactory agreement, in light of several approximations used in the theory. The somewhat larger values of the inelastic time τ_{in} obtained in the experiment could also be due to additional electron screening of the 2D electrons by X-electrons in AlAs/GaAs type-II superlattices.[19] Although the theory works for $kT > \hbar\omega_c$, Fig. 4.4 shows there is good agreement between the experiment and the theory (Eq. 4.1 and Eq. 4.2) at much lower temperatures ($kT \ll \hbar\omega_c$). Such correspondence does not appear for the magnetic field dependence of the width of the peak at the low temperatures discussed above (see curves at T=4.3 K and 2.3 K in Fig. 4.3). Thus, despite reasonable agreement between our experiments and the theory, additional investigations are required to understand the nonlinear response in the low temperature regime.

5. ZERO DIFFERENTIAL RESISTANCE STATE OF 2DEG ELECTRON SYSTEMS IN STRONG MAGNETIC FIELDS

5.1 Introduction

In accordance with the findings[10, 22] presented in the previous chapter the nonlinearity of the longitudinal resistance is strongly enhanced at low temperature due to a reduction in the electron-electron scattering needed to equilibrate the distribution function. A natural question arises: what will happen at low temperatures where the nonlinearity is so strong, that resistance drops very rapidly with electric field? In this chapter we investigate this question. We found that at low temperatures and at dc bias I_{dc} above a threshold value I_{th} the differential resistance of the 2D electron systems stabilizes suddenly near the value zero. In other words, for $I_{dc} > I_{th}$ the longitudinal dc voltage V_{xx} becomes independent of the dc bias. This is accompanied by a sharp dip in the differential resistance at the threshold bias. At higher bias, $I_{dc} > I_{th}$, temporal fluctuations of the differential resistance around the value zero are observed at low temperatures. The differential resistance is found to be positive again at very high bias where inter-Landau level transitions become important [5, 20, 22, 24, 25]. Our experiments thus demonstrate that in the presence of an electric field and strong

magnetic field, the 2D electron system undergoes a transition to a quasi-stationary state with zero differential resistance.

5.2 Sample and Experimental Setup

The samples studied in this research have a slightly low electron density than the ones used in the experiments presented in the previous chapters. The samples are cleaved from a wafer of a high-mobility GaAs quantum well grown by molecular beam epitaxy on semi-insulating (001) GaAs substrates. The width of the GaAs quantum well is 13 nm. Three samples (N1,N2,N3) are studied with electron density n_1=8.2 $\times 10^{15}$ (m^{-2}), n_2=8.4$\times 10^{15}$ (m^{-2}), n_3=8.1$\times 10^{15}$ (m^{-2}) and mobility μ_1=85 (m^2/Vs), μ_2=70 (m^2/Vs) and μ_3=82 (m^2/Vs) at T=2K. Measurements are carried out between T=0.3K and T=20 K in magnetic field up to 1 T on d=50 μm wide Hall bars with a distance of 250 μm between potential contacts. The differential longitudinal resistance is measured at a frequency of 77 Hz in the linear regime. Direct electric current (dc bias) was applied simultaneously with ac excitation through the same current leads (see inset to Fig. 5.1). All samples demonstrate similar behavior. We show data for sample N1 (except in Fig. 5.4).

5.3 Experimental Results

Dependence of the longitudinal resistance $r_{xx} = dV_{xx}/dI$ on the DC bias is presented in Fig. 5.1 at temperature T=0.3(K) and magnetic field B=0.784 (T). This magnetic

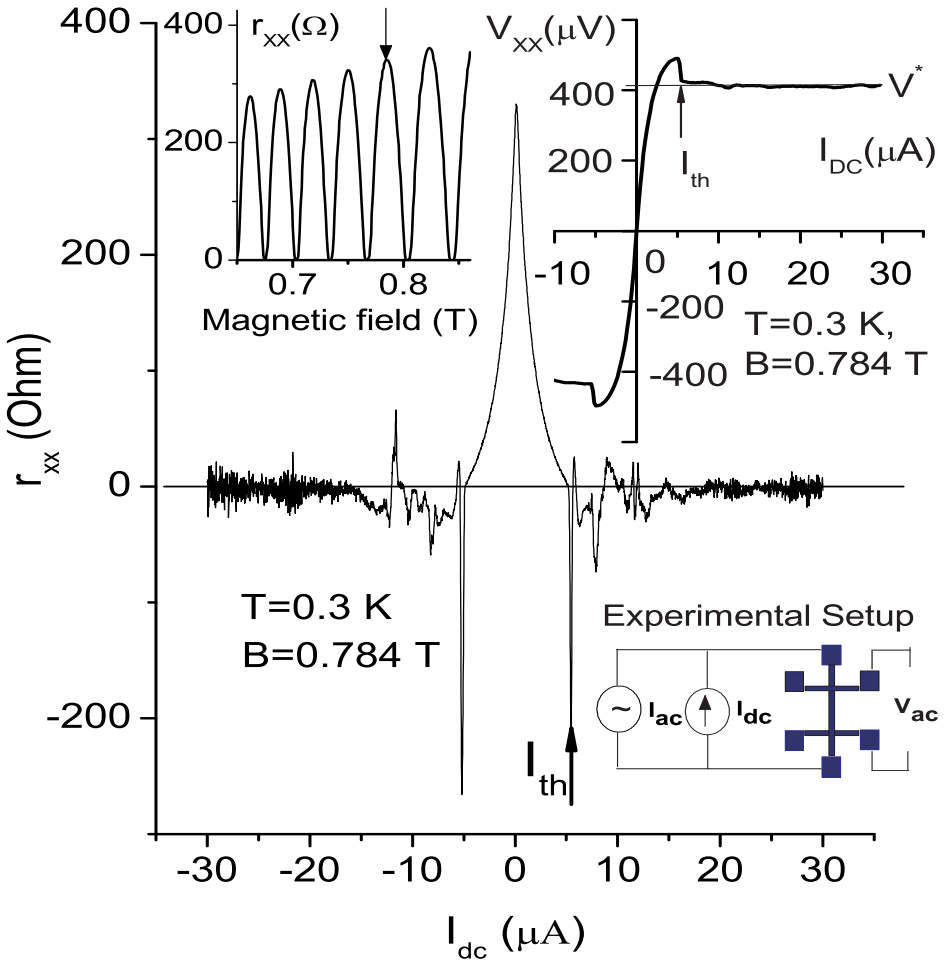

Fig. 5.1: The dependence of the differential resistance on dc bias at T=0.3K and the magnetic field B=0.784T marked by the arrow in the top left insert. The top left insert shows the linear resistance vs magnetic field at T=0.3K. The top right insert shows V_{xx} vs I_{dc} at T=0.3K and B=0.784T; the threshold bias I_{th} is designated by the arrow. The experimental setup is shown at bottom right.

field corresponds to the Shubnikov de Haas (SdH) oscillation maximum indicated by the arrow in the top left inset to the figure. For small dc bias the differential resistance decreases approaching zero. As the dc bias is raised further, the resistance exhibits a reproducible sharp negative spike at I_{th}=5.45 (μA), and then stabilizes near zero. At higher biases $I_{dc} > 15\mu A$ temporal fluctuations of the differential resistance are observed. The top right inset to the figure shows V_{xx} vs I_{dc} for the same experimental conditions. At $I_{dc} > I_{th}$ the longitudinal voltage V_{xx} stabilizes near a constant value V^*, in agreement with the behavior of the differential resistance r_{xx}.

Fig. 5.2a shows the dependence of r_{xx} on dc bias at different temperatures in a fixed magnetic field B=0.784T. The transition to the zero differential resistance state is observed at temperatures below 4K. At higher temperatures the differential resistance, although quite small, does not undergo a transition to the zero differential resistance state. A possible reason for this behavior is that the nonlinear response to dc bias is much weaker at higher temperatures due to increased inelastic scattering scattering [10, 22]. The weaker nonlinearity thus requires stronger dc bias for the same nonlinear change of resistance. The higher dc bias induces more inter-level scattering [5, 20, 22, 24, 25], increasing the longitudinal resistance.

The density of electron states is highest at SdH maximum and the high density of states enhances electron diffusion in energy space (spectral diffusion) providing a strong nonlinear response to the dc bias[10, 22]. Fig. 5.2b shows r_{xx} versus dc bias for different magnetic fields corresponding to SdH maximum. At T=2.16K the transition

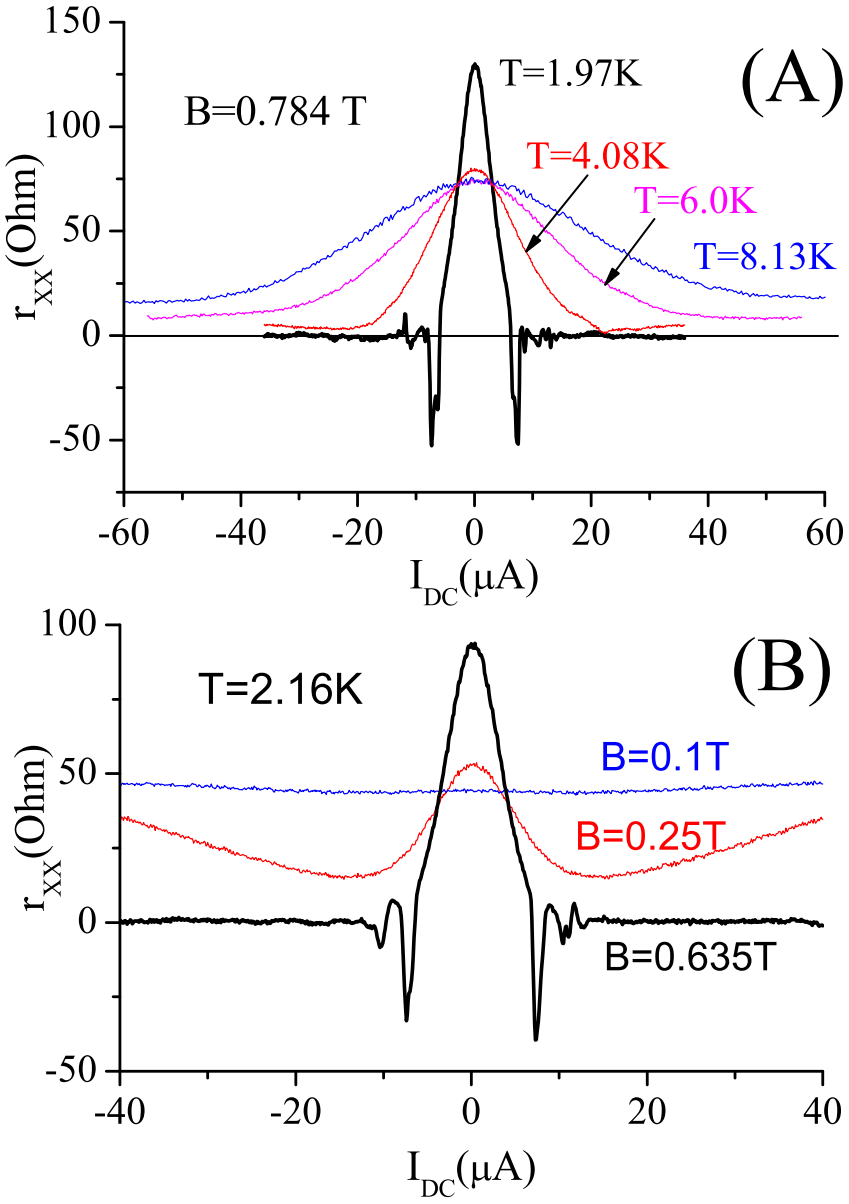

Fig. 5.2: a) Dependence of differential resistance r_{xx} on dc bias at different temperatures, as labeled; B=0.784 T. The zero differential state is observed at T=1.97K b) Dependence of differential resistance r_{xx} on dc bias at different magnetic fields, as labeled; T=2.16K. The zero differential resistance state is observed at B=0.635T

to the zero differential resistance state occurs at magnetic fields above B=0.4 (T). At lower magnetic field the differential resistance reaches a minimum positive value at a dc bias I_{min}. The resistance r_{min} increases with decreasing magnetic field[21]. This behavior can be attributed to several effects. One is related to the decrease of the modulation of the density of states with energy at low magnetic fields due to the overlap of Landau levels. The weak modulation of the density of states results in more uniform diffusion in energy space, causing a reduction in the magnitude of the oscillating non-equilibrium distribution function and the nonlinear conductivity [10, 22]. Another effect is the increase of the (bias induced) inter Landau level scattering due to the decrease of the Landau level separation at low magnetic field[5, 25]. Thus, a transition to the the zero differential resistance state occurs when there are substantial modulations of the coefficient of the spectral diffusion, weak inelastic relaxation and small inter-level scattering.

The longitudinal voltage V_{xx} is plotted as a function of I_{dc} in Fig. 5.3a for different temperatures in a magnetic field B=0.784T corresponding to a SdH maximum. V_{xx} depends strongly on temperature. As noted earlier, the transition to the zero differential resistance state occurs for temperatures below 4 K, where V_{xx} tends toward a constant value V^* at sufficiently high currents I_{dc}. The value of V^* at high bias varies with temperature above 2 K and tends toward a value that is independent of temperature below 2 K. The $V_{xx} - I_{dc}$ curves in Fig. 5.3b taken at magnetic fields corresponding to different SdH maximum indicate that the longitudinal voltage V^*

also varies with magnetic field. At very high dc bias the inter-level scattering becomes important and the system returns to a state with positive differential resistance. This is shown in Fig. 5.4a.

5.4 Discussion of the ZRS states in the Samples

To the best of our knowledge, the zero differential resistance state is a new, strongly nonlinear state of 2D electron systems under dc bias in high magnetic field. The state has not been observed before in studies of highly mobile electrons [9, 21, 20, 22, 24]. A possible reason is, that in our lower mobility samples the *stronger* transport scattering $1/\tau_{tr}$ stimulates more effective spectral diffusion and, therefore, the stronger nonlinearity. This point is also supported by recent experimental observation of the microwave induced ZRS in low mobility 2DEG [26]. Thus, very high mobility samples may not exhibit the strongest nonlinear response.

Although the dominant mechanism of the nonlinearity in the two dimensional electron systems in strong magnetic fields becomes to be more apparent, the experimental study of the strongly nonlinear stationary states of the 2D electron systems require additional efforts. There are several theories [16, 28, 29, 32, 51] that have analyzed the stability of non-equilibrium 2D electron systems in magnetic field. In this paper we use the approach developed by Andreev *et al.*[16]. Assuming the local relation $\vec{E} = \rho(J^2)\vec{J}$ between electric field $\vec{E}$ and current density $\vec{J}$ and taking into account

continuity and Poisson's equations, the stability conditions were found to be [16]:

$$\rho_{xx}(\mathbf{J}^2) \geq 0 \tag{5.1}$$

$$\rho_{xx}(\mathbf{J}^2) + \alpha \mathbf{J}^2 \geq 0 \tag{5.2}$$

,where ρ_{xx} is longitudinal resistivity and $\alpha = 2(\frac{d\rho_{xx}(\vec{J}^2)}{d\vec{J}^2})$.

In our case the longitudinal resistivity is positive $\rho_{xx} > 0$ at the transition. To analyze the second condition for stability (Eq. 5.2) we note that $\rho_{xx} = E_x/J$ and $\frac{d\rho_{xx}}{dJ} = 2J\frac{d\rho_{xx}}{d(J^2)}$, where E_x is longitudinal component of the electric field $\vec{E}$. With these relations Eq. 5.2 can be rewritten in the following form:

$$\rho_{xx}^{diff} = dE_x/dJ \geq 0 \tag{5.3}$$

where ρ_{xx}^{diff} is the longitudinal differential resistivity. The longitudinal differential resistance r_{xx} differs from ρ_{xx}^{diff} by a geometric factor γ (in our samples γ=5): $r_{xx} = \gamma\rho_{xx}^{diff}$. Thus, according to Eq. 5.2, the 2D electron system is unstable at negative differential resistance, $r_{xx} < 0$. Our experiments demonstrate there is a transition to the zero differential resistance state at $r_{xx} = 0$, in complete agreement with this theory [16]. We note also that the stability condition $r_{xx} \geq 0$ is quite general and has been used to analyze a broad set of instabilities, in particular the Gunn effect[31].

It is known from the Gunn effect [30, 31] that the instability of the homogeneous state at $r_{xx} < 0$ leads to the formation of electric domains moving through the

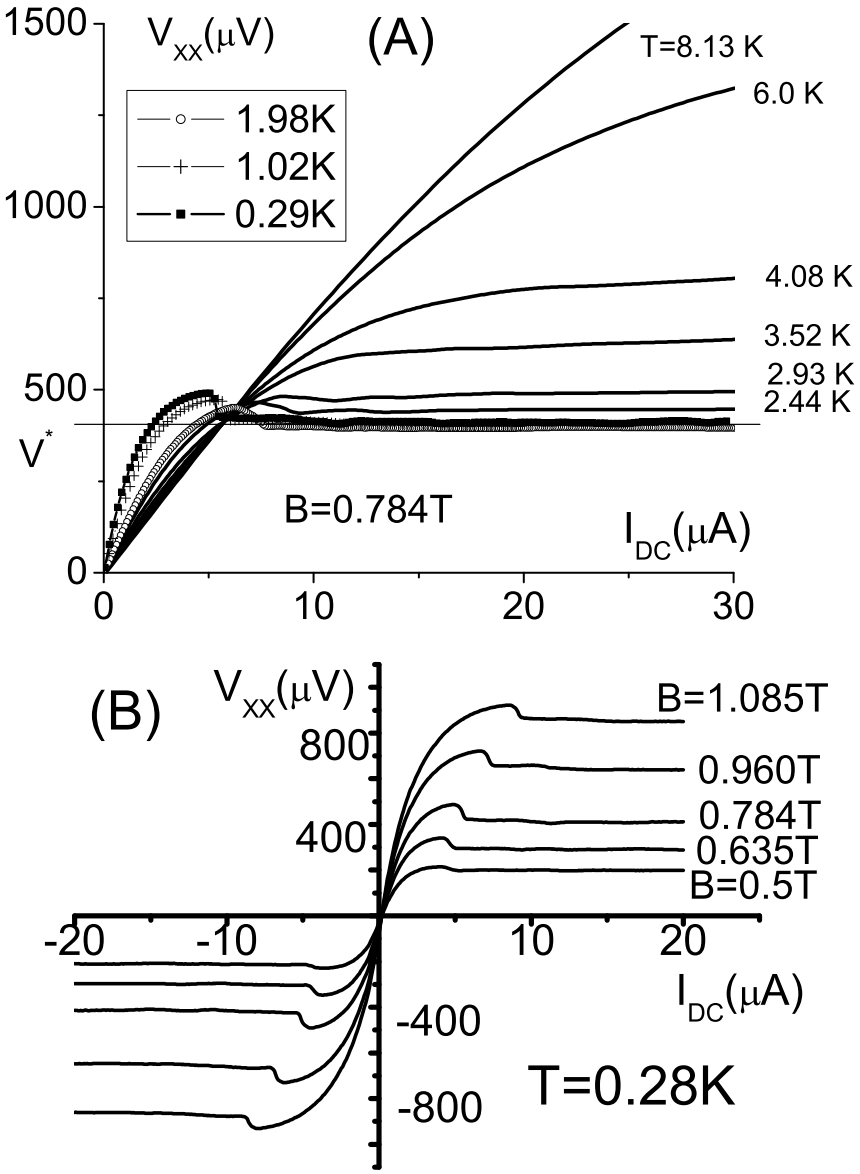

Fig. 5.3: (A) Dependence of the longitudinal voltage V_{xx} on dc bias I_{dc} at different temperatures as labeled; (b) V_{xx} versus I_{dc} at different magnetic fields (as labeled) corresponding to different SdH maximum.

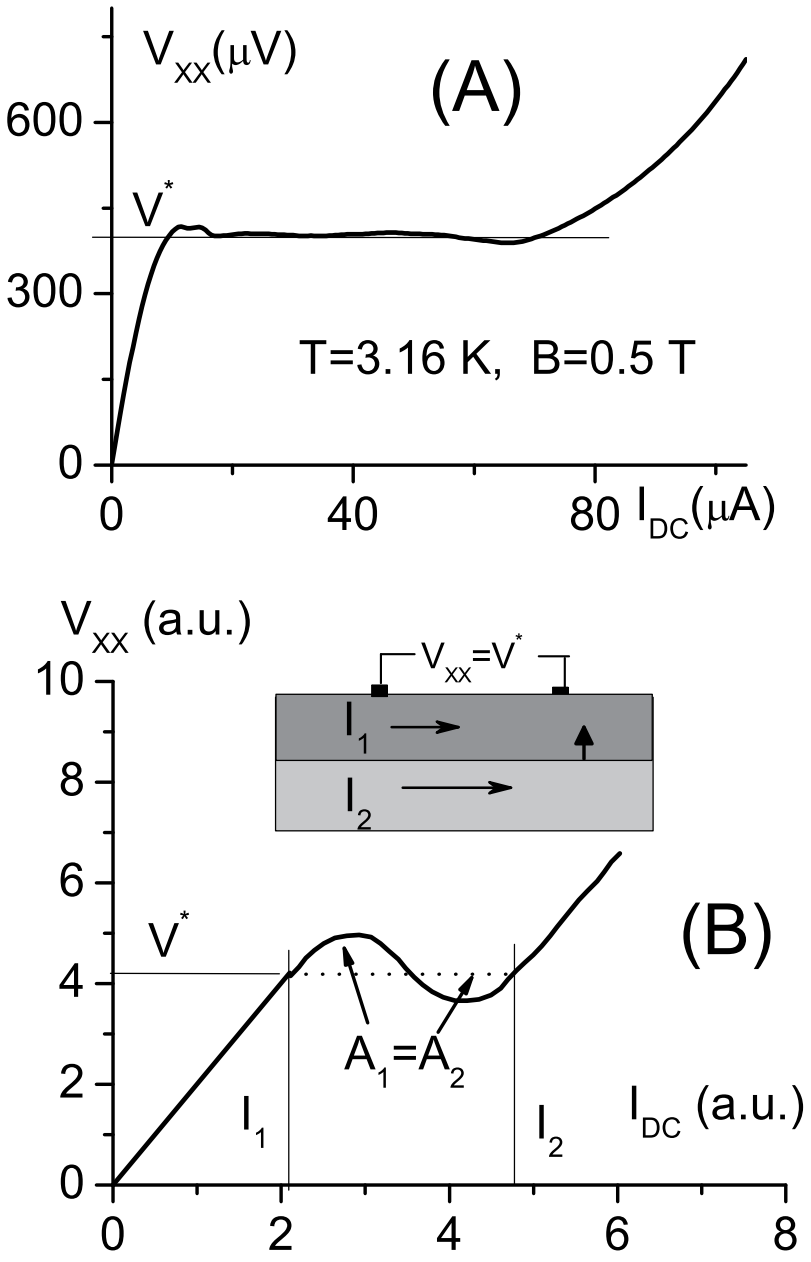

Fig. 5.4: (A) Dependence of the longitudinal voltage V_{xx} on dc bias for a wide range of bias (data for sample N3). (B) Proposed N-shaped $V_{xx} - I_{dc}$ dependence shows two values I_1 and I_2 with the same longitudinal voltage V^* determined by the equal-area rule: $A_1 = A_2$[30]. The insert illustrates a possible current distribution in a Hall bar geometry. The boundary between the two regions with homogeneous currents I_1 and I_2 moves from one side of the sample to the other with velocity $v_b = E_x^*/B$, where E_x^* is the longitudinal electric field at $I_{dc} > I_{th}$.

sample. Possible 2D domain structures have been considered recently[32] where the electric current and the Hall electric field are bistable. In the Hall bar geometry, two parts of the sample carry stable currents I_1 and I_2 with the same longitudinal voltage V^* as shown in the Fig. 5.4b. The horizontal boundary between these two regions must carry additional electrical charge, as the Hall electric field E_H changes in a step-like fashion across the boundary. Due to the presence of the longitudinal electric field $E_x^* = V^*/L$ (L is distance between potential contacts) the electrically charged boundary is not stationary and propagates across the sample with velocity $v_y = [E_x^* \times B]/B^2$. Thus, the electric current $I(t)$ oscillates in time with an average value equal to the dc bias: $< I(t) >= I_{dc}$. At the same time, the longitudinal voltage V_{xx} is independent of the dc bias I_{dc} and is determined by the rule of equal areas ($A_1 = A_2$) see Fig. 5.4b) [30].

6. DIRECTED ELECTRON TRANSPORT THROUGH BALLISTIC QUANTUM DOT UNDER MICROWAVE RADIATION

6.1 Introduction

A quantum dot is made from a semiconductor nanostructure that confines the motion of charged carriers in all three spatial directions. There are several types of confinement based on different technologies. An important restriction is due to electrostatic potentials generated by external electrodes, strain, doping, impurities etc. Due to very limited spatial size, a quantum dot has a discrete quantized energy spectrum. The corresponding wave functions are spatially localized within the quantum dot, but extend over many periods of the crystal lattice. A quantum dot contains a small finite number of charged carriers. The transport through quantum dots is shown to be heavily influenced by their spatial structure.

Nonlinear directed transport in mesoscopic objects is the subject of considerable fundamental interest because of potential applications in nanoelectronics. At high frequency, the unavoidable breaking of the inverse symmetry of small quantum systems by an impurity potential is reflected in photovoltic effects[39, 41, 43, 42, 40]. More recently, various competing mechanisms of rectification in quantum dots have been

proposed [32, 45, 42, 44, 43]and found experimentally [45]. Most efforts have been focused on the nonlinear properties of mesoscopic objects in the regime where the electron transport is governed by quantum interference. In this chapter we study nonlinear electron transport in a different regime, where classical ballistic trajectories appear to provide the dominant contribution to rectification. In the presence of magnetic fields, we have observed a gigantic reduction of the directed electron transport through a ballistic dot with a lateral size $d \approx 1\mu$ significantly smaller than the mean free path $l_p = 8\mu$ of the 2D electron gas in adjoining 2D layers.

6.2 Sample and Experiment Setup

The dot is fabricated from high mobility GaAs/AlGaAs heterostructures using electron beam lithography and consecutive plasma etching. The electron density n and mobility μ of the 2DEG are $n = 3.08 \times 10^{11}\text{cm}^2$ and the $\mu = 0.91 \times 10^6\text{cm}^2/\text{Vs}$. A schematic view of the sample is presented in Fig. 6.1. The dot is restricted by boundaries of three insulating disks of diameter 5μ etched inside the 2D conducting layer [see Fig. 6.1b].Three narrow leads (left, right, and top conducting channels) with a width approximately 0.3μ, formed by the discs, provide electrical connections between the dot and three electrically isolated macroscopic 2D electron systems. In order to change the dot resistance a semitransparent metal gate is placed on top of the structure at a distance 86 nm above the 2D electron gas.

Measurements were done in vacuum chamber of an He-3 insert at a temperature 0.3

-6K and a magnetic field up to 2T. Microwave radiation (1-40 GHz) is applied through a semirigid coaxial cable terminated by a parallel two-wire line. The line is placed at 3-5 mm above the sample. The electric field of microwaves is oriented along an edge of the sample as shown in Fig. 6.1a. The resistance of the dot (and the 2D electron systems) is determined by standard 4- points method at frequency 10 Hz in the linear regime. The rectified voltage is measured using high impedance digital multimeters.

6.3 Experiment Results

Linear properties of the dot are shown in Figs. 6.1c and 6.1d. Fig. 6.1c illustrates the dependence of the dot conductance on the top gate voltage at different current voltage configurations. The data in Fig. 6.1c show that there is good conductance through the horizontal leads ($\sigma_{5d,34}$), while the conductance $\sigma_{sd,23}$ through the vertical contact with slightly less width is small, especially at low gate voltages $V_g \approx -0.08V$. At low gate voltages the conductance $\sigma_{sd,23}$ demonstrates an activated dependence on temperature indicating the lack of conducting channels in the vertical lead. The conductance $\sigma_{5d,34}(-0.08V) \approx 3e^2/h$ through the horizontal channels remains roughly same between $T = 1$ and 6 K. At lower temperatures the gate voltage causes reproducible conductance oscillations reported earlier [33]. The magnetic field dependence of the conductance $\sigma_{sd,23}$ is shown in Fig. 6.1d. Conductance increases by a factor 1.5 to 2 in the magnetic field up to 2 T and displays quasiperiodic oscillations observed in ballistic dots [33, 46].

Rectification of microwave radiation by the quantum dot is shown in Fig. 6.2a. The rectified voltage V_{2-3} is measured between contacts 2 and 3 [see Fig. 6.1a]. One of the main properties of rectification is a very strong dependence on the magnetic field. The reduction of rectification by 2 orders of magnitude is observed in the magnetic field $H > 0.5$ T at the dot conductance $G_{sd,23}$ below e^2/h. This decrease is much stronger than variations of the dot conductance $G_{sd,23}$ with the magnetic field [see Fig.

6.1d]. At higher dot conductance the rectified voltage V_{2-3} is smaller [upper curves on Fig. 6.2a]. A negligibly small rectified voltage V_{4-3} is found between contacts 4 and 3 (not shown). Fig. 6.2d demonstrates the dependence of microwave rectification on gate voltage V_g at three different magnetic fields: $H = 0$, $+0.56$ T, and -0.56 T. The strong reduction of directed electron transport by the magnetic field is observed in a broad range of gate voltages.

At the same time the dot conductance $\sigma_{sd,23}(V_g)$[Fig. 6.2b] and its logarithmic derivative $d[\ln \sigma_{sd,23}]/dV_g(V_g)$[Fig. 6.2c] are not changed considerably by the magnetic field. We estimate a scale of magnetic fields essential for rectification by measuring the width W of the first curve in Fig. 6.2a at half maximum (marked by a horizontal line in the figure). The half-width $W/2 = 0.088$T is close to field $H = 0.085$ T at which the cyclotron radius $r_H$of electrons at the Fermi level is equal to the dot size d. Thus, the directed transport is reduced by half of its zero field efficiency at the magnetic field corresponding to the condition $r_H \approx d$. This is strong evidence for a ballistic origin of the microwave rectification.

Fig. 6.3 presents an evolution of the magnetic field dependence of the rectification with the microwave frequency. The component symmetric (antisymmetric) with respect to magnetic field is shown in the left (right) panel. While the antisymmetric part of the directed transport is quite similar for different frequencies, the symmetric component shows a significant change in the magnetic field dependence for microwave frequencies above 10 GHz. An additional structure occurs at the microwave frequen-

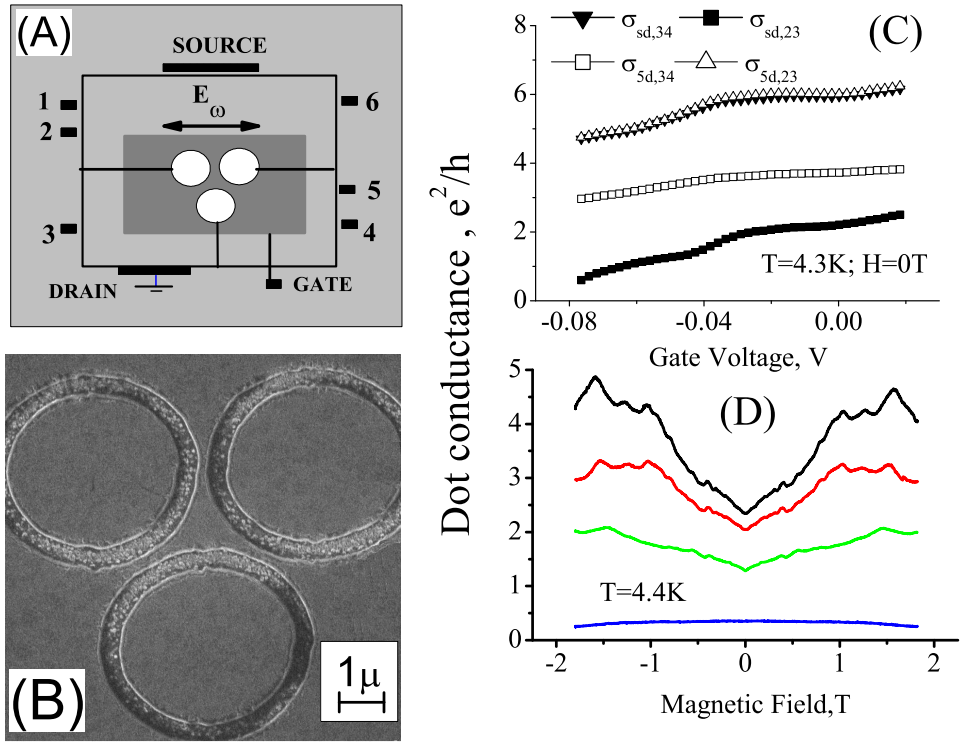

Fig. 6.1: Left panel: (A) Dependence of the dot conductance $G_{sd,23}$ on the gate voltage, H=0T. (B) Dependence of the dot conductance $G_{sd,23}$ on perpendicular magnetic field. Different curves corresponds to different gate voltages (from bottom to top in mV): -80.8, -52.9, -29.3, 0. Right panel: Dependence of the rectified voltage $V_{2,3}$ on magnetic field at the same gate voltages as on the plot (B). Sign of the rectified voltage corresponds to electrons pumping into 2D area connected to contacts 1,2 and the source.

cies above 10-15 GHz, changing the direction of the rectified transport at zero magnetic field. The physical parameters relevant to the temporal behavior of the quantum dot are level spacing: $\Delta = 2\pi\hbar^2/(m^*A) = 28$ mK, bulk momentum relaxation time: $\tau_p = 34$ ps and time of ballistic electron flight across the dot$\tau_f \approx 2d/V_F = 10$ (ps). Thus, Fig. 6.3 reveals that, if the microwave period $\sim 1/\omega$ is comparable or shorter than the time of ballistic electron flight τ_f: $\omega\tau_f \geq 1$, then significant changes of the directed transport through the dot occurs. Again, it points toward the ballistic origin of rectification.

At zero magnetic field the rectified voltage increases by 10%-20% with the temperature decrease from 6 K down to 1 K at $\sigma_{sd,23} \approx e^2/h$. The weak temperature dependence is in agreement with the ballistic origin of rectification.

Below we discuss the mechanisms of rectification. One of the simplest mechanisms is related to the modulation of dot conductance induced by microwave oscillations of the gate voltage V_g. During the first half of the microwave period, when the dot conductance is big, the microwave current through the dot is stronger than the current during the second half of the period, when the dot conductance is small. At small modulations the net direct current (average over the microwave period) is proportional to the first derivative of the dot conductance σ to the gate voltage V_g : $I_{\rm rect} = A[d\sigma/dV_g]V_\omega^2$, where V_ω is microwave voltage applied to the dot and A is a constant. The rectified voltage $V_{\rm rect}$ equals $V_{\rm rect} = I_{\rm rect}/\sigma$. Thus $V_{\rm rect} = A[(d\sigma/dV_g)/\sigma]V_\omega^2$ is proportional to the logarithmic derivative $[d(\ln\sigma)/dV_g]$ of the

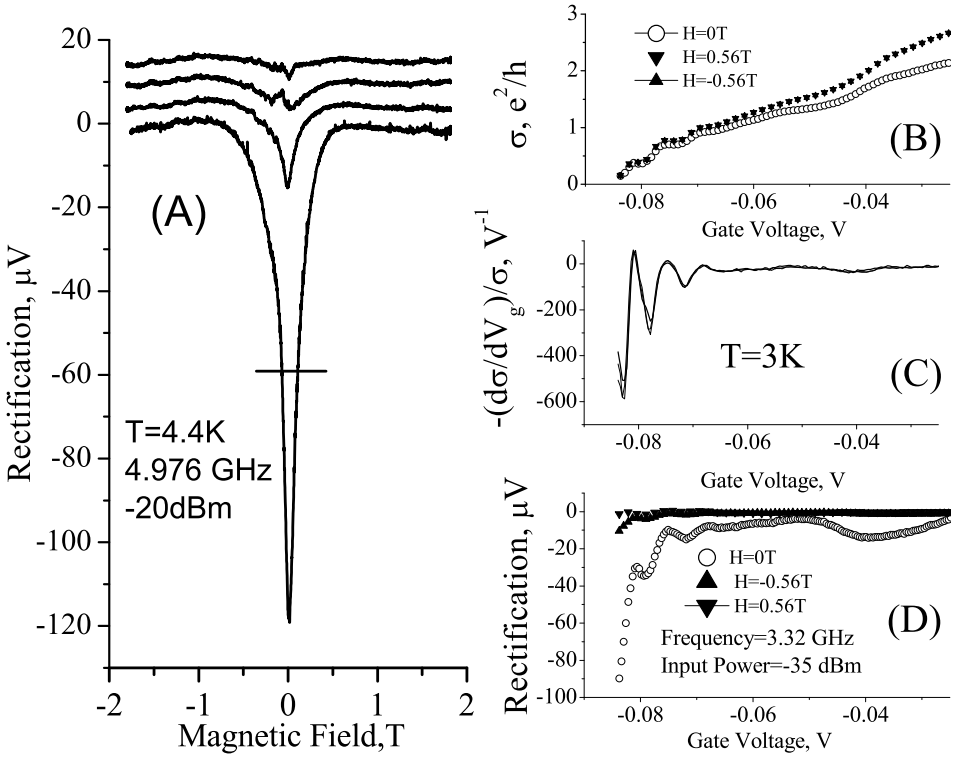

Fig. 6.2: Left panel: Dependence of the rectification on microwave power at different magnetic filed as labeled. The dot resistance $R_{sd,23}$ is 25 KOhm. Right panel: dependence of the rectification on microwave power at different dot resistance at zero magnetic field. Sign of the rectification is inversed.

dot conductance.

The dot conductance σ, its logarithmic derivative $[d(\sigma)/dV_g]/\sigma$, and the rectified voltage $V_{\rm rect}$ versus the gate voltage are shown on Figs. 6.2b-d, respectively. Although some correlations exist, there is a significant difference between the curves presented in Figs. 6.2c and 6.2d. The microwave rectification [Fig. 6.2d] is quite efficient at $V_g \approx -0.08$ V and -0.073 V at which the conductance [Fig. 6.2b] shows a plateaulike behavior and the gate modulation of the dot conductance is negligibly small [Fig. 6.2c]. Moreover, the strong reduction of rectification by the magnetic field in Fig. 6.2d is in apparent contradiction with a very small (almost unrecognizable) effect of the magnetic field on the logarithmic derivative in Fig. 6.2c. Thus, experiments indicate that microwave modulation of the dot conductance is not the main mechanism of dot rectification.

Below we suggest a different mechanism of rectification. Figure 6.2 demonstrates that electron trajectories with a length l, which is no shorter than the dot size $d (l \geq d)$, provide the main contribution to the rectification. Shorter trajectories with $l < d$, which are changed considerably by stronger magnetic field ($H > 0.088$ T), do not provide any significant contribution to the rectification: $V_{\rm rect}(H > 0.088T) \sim 0$. On the other hand, Fig. 6.3 demonstrates that trajectories, which are not much longer than the size of the dot, are important. To understand it, we consider an electron with Fermi velocity v_F propagating along a trajectory with length l during time $t_p = l/v_F$. If microwaves with low frequency $\omega t_p \ll 1$ are applied, the electron sees a

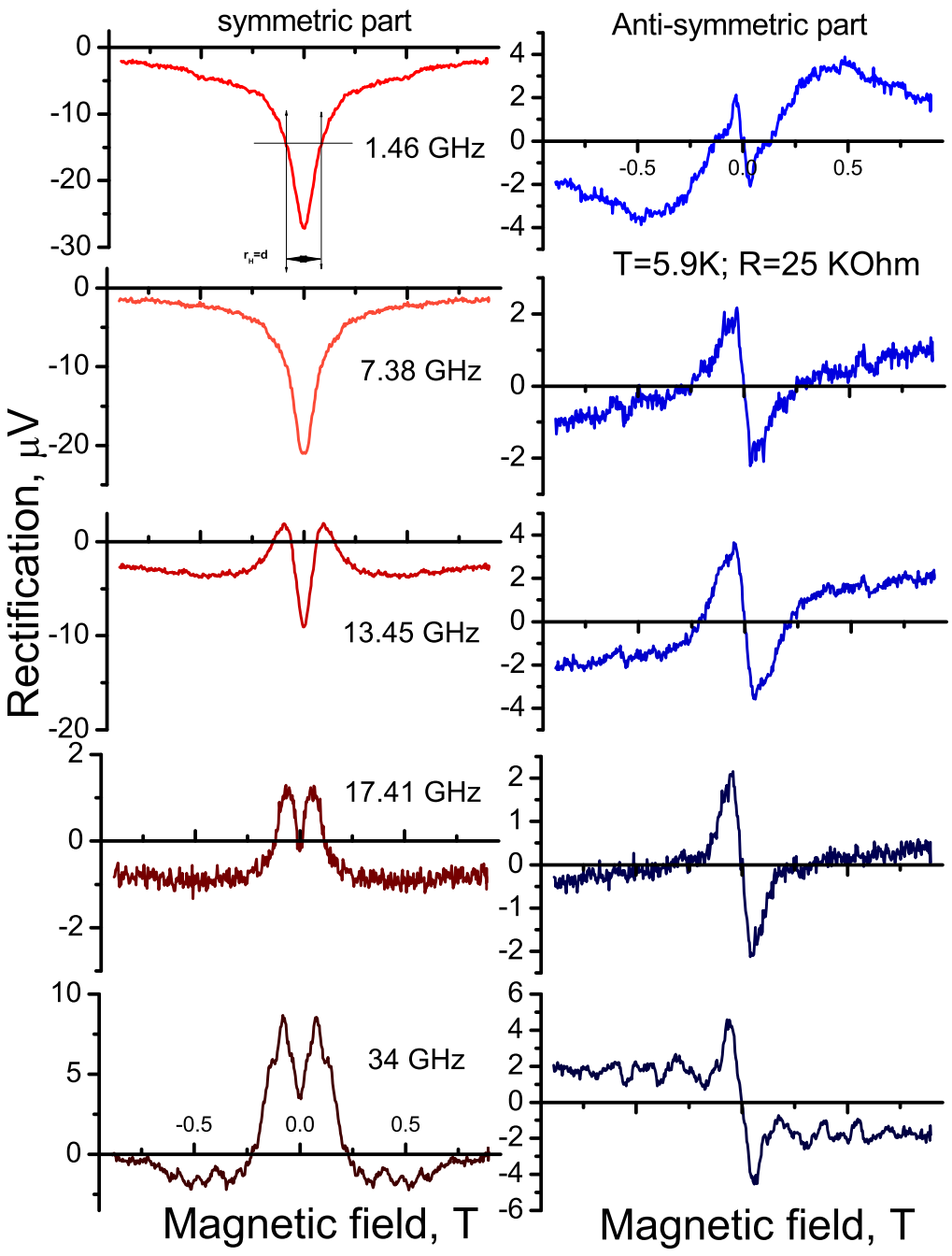

Fig. 6.3: Rectified voltage vs magnetic field at different microwave frequencies as labeled. Different microwave power for different curves. Perturbative regime: $V_{\rm rect}$ ∼power. Form of the curves does not depend on the power. Left panel presents symmetric part of the magnetic field dependence. Right panel presents asymmetric part. T=5.9K, R=25KOhm.

quasistationary electric field. At high frequency $\omega t_p \gg 1$, the electric field oscillates during time t_p, and as a result the accumulative effect of the high frequency field on electron motion is significantly different from the low frequency case. The crossover from one regime to another occurs at frequency $\omega t - p \approx 1$. In the experiment the crossover occurs at frequency $\omega_{cr}/2\pi \approx 10 - 15$ GHz $[t_p = 1/\omega_{cr} \approx 10 - 15(\text{ps})]$, indicating, that the trajectories with length $l \leq 2d - 3d$ are essential for microwave rectification. Thus the data in Figs. 6.2 and 6.3 demonstrate that electron trajectories with lengths comparable with the dot size $l \sim d$ are most effective for rectification. We refer to it below as $effective$ trajectories (electrons).

Let us consider an equilateral triangular dot with three conducting leads placed at its corners: top, left, and right, and with a microwave electric field $\vec{E}_\omega(r)$ applied across the dot. The microwaves create a voltage V_ω between left and right leads. Because of the long mean free path $lp \gg d$, the linear response to the electric field $\vec{E}_\omega(r)$ is nonlocal: the electric current $I(r)$ at a position r inside the dot is determined by all electron trajectories coming to this point r, which have been exposed by the microwave electric field $E_(r')$ at a different point r' inside the dot. Most likely the direction of an electron motion along a particular trajectory $\vec{x}(t)$ at the point r is different from the direction of the electric field $\vec{E}_\omega(r)$ at the same point r.

For each electron trajectory $\vec{x}(t)$ the electric field $\vec{E}_\omega(r)$ can be decomposed on normal $E^\perp(r)$ and tangential $E^\parallel(r)$ to the trajectory components.

The tangential component $E^\parallel(r)$ changes the energy (speed) of the effective electrons

$\delta\epsilon = p_F \delta v_{l,(r)} = \int E^{\parallel}(r) dx_{l,(r)} = \pm\alpha V_\omega$, where p_F is the Fermi momentum, α is a constant, and $\delta v_{l,(r)}$ is the change of the speed of the effective electrons ejected from the left (right) lead. The sign "+(-)" corresponding to the velocity $v_l(v_r)$ is a result of dot symmetry. The normal component $E^{\perp}(\vec{x})$ changes the direction of the velocity of the effective electrons and, as a result, bends the effective trajectories $\vec{x}_{l,(r)}(t)$. The ejection of electrons from the hornlike leads [see Fig. 6.1a] is substantially anisotropic and, therefore, the bending changes the density $n_l(n_r)$ of the effective electrons coming from the left (right) channel to the top lead. At a small bending the change of the density $n_l(n_r)$ is proportional to the amplitude of the microwave electric field: $\delta n_{l,(r)} = \pm\beta V_\omega$, where β is a constant. The sign "+(-)" corresponding to the density $n_l(n_r)$ is a result of the dot symmetry. The rectified current through the top lead is found to be

$$I_{\rm rect} = e\delta n_l \delta v_l + e\delta n_r \delta v_r = (2\alpha\beta/p_F) V_\omega^2 \tag{6.1}$$

An important property of the proposed mechanism is a natural sensitivity of the directed transport to the magnetic field. A strong magnetic field ($H > 0.085$ T) affects substantially the effective trajectories with $l \sim d$, forcing the effective electrons to perform a cyclotronlike, circular motion inside the dot. It should reduce significantly the electron flux transported by the effective trajectories between the leads. Another important outcome from the suggested picture is a natural sensitivity of the rectification to the microwave frequency. At high microwave frequency ($\omega\tau_f \gg 1$) the

rectification should be less effective, because of a significant decrease of speed variations of the effective electrons:$\delta v \sim \int eE^{\parallel}(x,t)dx \sim 1/\omega\tau_f$as well as due to a reduction of the electron bending in the high frequency microwave field. Observable changes of rectification should be detectable at $\omega\tau_f \approx 1$, corresponding to the experiment (see Fig. 6.3).

7. SUMMARY

In summary, the nonlinear properties of low dimensional electron gas at low temperatures are the focus of this thesis. Several new phenomena have been observed in our experiments.

In the beginning, for the samples of highly mobile two dimensional gas, we found that strong oscillations of the resistance are periodic in inverse magnetic fields in DC biased samples. The position of the oscillation maximums is found to be proportional to the DC density. Similar oscillations are observed with AC excitations applied to the samples at different frequencies ranging from 10 KHz to 20 GHz. We have shown that the oscillations in the resistance observed at frequencies below 100 KHz are due to the non-linear response of the DC biased two dimensional electron systems.

Further investigations revealed that at small dc bias a strong reduction of the longitudinal resistivity is not related to Joule heating even at temperatures down to 2K, where strong quantum oscillations (SdH) are present that are highly sensitive to the temperature. At low temperature (2-10K), the scale of the electric fields at which the effect occurs is proportional to the temperature. In the high temperature regime, $kT > \hbar\omega_c$, reasonable agreement is established with recent theory[10] that has

predicted significant and nontrivial variations of the electron distribution function in response to a DC electric field. Comparison with the theory allowed us for the first time to obtain the inelastic electron-electron scattering time τ_{in} in the presence of magnetic fields, and the quantum scattering time τ_q of the two dimensional electron systems at high temperatures.

Additional study demonstrated a zero differential resistance state $r_{xx} = 0$ in two-dimensional electron systems above a threshold value I_{th} of dc bias I_{dc} in the presence of strong magnetic fields at low temperatures. The transition to this state is accompanied by a sharp dip of the differential resistance. Temporal fluctuations of the longitudinal resistance are observed for $I_{dc} > I_{th}$ at the lowest temperatures(0.3K). We have suggested that the quasi-stationary nonlinear electron state forms due to local instability of the electric current at $r_{xx} < 0$. The instability is stimulated by strong spectral diffusion of the electrons induced by the Hall electric field. This suggestion is supported by an analysis of the stability of two dimensional electron systems in a magnetic field.

Finally, in the research of a zero dimensional sample, a ballistic quantum dot, an unexpected gigantic reduction of directed electron transport through the ballistic quantum dot under microwave radiation is observed in magnetic fields, at which the electron cyclotron radius at the Fermi level r_H is smaller than the lateral size of the dot d: $r_H \leq d$. The effect exists in a broad range of the dot conductances and depends weakly on temperature. Rectification varies significantly with microwave frequency

ω above 10-15 GHz, at which the period of microwave oscillations is comparable with the time τ_f of the ballistic flight through the dot. A ballistic model of the directed transport is proposed.

BIBLIOGRAPHY

[1] N. W. Ashcroft, N. D. Mermin, Solid State Physics, Holt, Rinehart and Winston, 1976.

[2] Supriyo. Datta, Electronic transport in mesoscopic systems, Cambridge university press, 1995.

[3] J. M. Ziman, Principles of the theory of solids, Cambridge at the university press, 1972.

[4] T. Ando, A. Fowler and F. Stern, Rev. Mod. Phys. **54**, 437(1982).

[5] C. L.Yang, J. Zhang, and R. R. Du, J. A. Simmons and J. L. Reno, Phys. Rev. Lett. **89**, 076801 (2002).

[6] M.A. Zudov, R. R. Du, J. A. Simmons, and J. L. Reno, Phys. Rev. B **64**, 201311(R) (2001); P.D. Ye, L. W. Engel, D.C. Tsui, J. A. Simmons, J. R. Wendt, G. A. Vawter, and J. L. Reno, Appl. Phys.Lett. **79**,2193 (2001).

[7] C. L. Yang, M. A. Zudov, T. A. Knuuttila, R. R. Du, L. N. Pfeiffer and K. W. West, Phys. Rev. Lett. **91**, 096803 (2003).

[8] R. G. Mani, V.Narayanamurti, K. vonKlitzing, J. H. Smet, W. B. Jonson, and V. Umansky, Nature(London) **420**, 646 (2002).

[9] R. G. Mani, V. Narayanamurti, K. von Klitzing, J.H. Smet, W.B. Jonson, and V. Umansky Phys. Rev. B **70**, 155310 (2004).

[10] I. A. Dmitriev, M.G. Vavilov, I. L. Aleiner, A. D. Mirlin, and D. G. Polyakov, Phys. Rev. B **71**, 115316 (2005).

[11] M. G. Vavilov and I. L. Aleiner Phys. Rev. B **69**, 035303 (2004).

[12] I. A. Dmitriev, A. D. Mirlin and D.G.Polyakov, Phys. Rev. Lett. 91, 226802 (2003).

[13] M.A. Zudov, R. R. Du, L. N. Pfeiffer, and K. W. West, Phys. Rev. Lett **90** 046807 (2003).

[14] R. L. Willett, L. N. Pfeiffer, and K. W. West, Phys. Rev. Lett **93** 026804 (2004).

[15] A. C. Durst, S. Sachdev, N. Read, and S. M. Girvin, Phys. Rev. Lett. **91**, 086803 (2003).

[16] A. V. Andreev, I. L. Aleiner, and A. J. Millis, Phys. Rev. Lett. **91**, 056803 (2003).

[17] P. W. Anderson and W. F. Brinkman, cond-mat/0302129.

[18] J. Shi and X. C. Xie, Phys. Rev. Lett. **91**, 086801 (2003).

[19] K. J. Friedland, R. Hey, H. Kostial, R. Klann, and K. Ploog, Phys.Rev.Lett. **77**, 4616 (1996).

[20] A. A. Bykov, Jing-qiao Zhang, Sergey Vitkalov, A. K. Kalagin, and A. K. Bakarov Phys. Rev. B **72**, 245307 (2005).

[21] A. A. Bykov, A. K. Kalagin,an d A. K. Bakarov JETP Lett. **81**(2005).

[22] Jing-qiao Zhang, Sergey Vitkalov, A. A. Bykov, A. K. Kalagin,and A. K. Bakarov Phys. Rev. B **75** (2007).

[23] http: //www.bell-labs.com/jc-cond-mat/september/september_2006.html

[24] W. Zhang, H.-S. Chiang, M. A. Zudov, L.N. Pfeiffer, and K.W. West, Phys. Rev. B **75**, 041304(R) (2007).

[25] M.G. Vavilov, I.L Aleiner, and L.I. Glazman, cond-mat/0611130.

[26] A. A. Bykov, A. K. Bakarov, D. R. Islamov, A. I. Toropov, JETP Letters **84**, 391 (2006).

[27] A. A. Bykov, Jing-qiao Zhang, Sergey Vitkalov, A. K. Kalagin, and A. K. Bakarov, Phys. Rev. Lett. **99**, 116801 (2007).

[28] A. Auerbach, I Finkler, B. I. Halperin, and A. Yacoby, Phys. Rev. Lett. **94**, 196801 (2005).

[29] A. Auerbach and G. Venketeswara Pai, arXiv:cond-mat/0612469.

[30] P.N. Butcher, Phys. Lett. **19**, 546 (1965).

[31] V.L. Bonch-Bruevich, S.M. Kogan, Sov. Phys. Solid-State **7**, 15 (1965).

[32] M. G. Vavilov and I. L. Aleiner, Phys. Rev. B **64**, R16311 (1999).

[33] J. P. Bird , R. Akis, D. K. Ferry, A. P. S. de Moura, Y-C. Lai and K. M. Indlekofer, Rep. Prog. Phys. **66** 583 (2003).

[34] J. P. Bird, R. Akis, D. K. Ferry, D. Vasileska, J. Cooper, Y. Aoyagi, and T. Sugano, Phys. Rev. Lett. **62** 2523(1989).

[35] J. P. Bird and M. Stopa *et al*, Phys. Rev. B **56**, 7477 (1997).

[36] R. Akis, J. P. Bird and D. K. Ferry, Appl. Phys. Lett. **81** 129(2002).

[37] M. Büttker, Phys. Rev. B **51**, 7010(1995).

[38] A. M. Song, A. Lorke, A. Kriele, and J. P. Kotthaus, Phys. Rev. Lett. **80**, 3831(1998).

[39] D. Thouless, Phys.Rev. B **27**,6083 (1983).

[40] V. I. Falko and D. E. Khmel'nitskii, Zh.Eksp.Teor.Fiz. **95**,328 (1989) [Sov. Phys.JETP **68**, 186 (1989)].

[41] A.A.Bykov *et al.*, Pis'ma Zh.Eksp.Teor.Fiz. **49**, 13, (1989) [JETP Lett., **49**, 13 (1989)].

[42] B. Spivak *et al.* Phys. Rev. B **51**, 13226 (1995).

[43] P.W. Brouwer, Phys.Rev. B **58**, R10135 (1998).

[44] T.A. Shutenko, I.L. Aleiner, and B.L. Altshuler, Phys. Rev. B **61** 10366(2000).

[45] L. DiCarlo, C. M. Marcus and J. S. Harris, Jr., Phys. Rev. Lett, **91**, 246804 (2003).

[46] P. Boggild, A. Kristensen, H. Bruus, S.M. Reimann, and P.E. Lindelof, Phys. Rev. B, **57**, 15408 (1998).

[47] P.D. Ye, L. W. Engel, D.C. Tsui, J. A. Simmons, J. R. Wendt, G. A. Vawter, and J. L. Reno, Appl. Phys.Lett **79**,2193 (2001).

[48] S. I. Dorozhkin, JETP Lett. **77**, 577 (2003).

[49] S. I. Dorozhkin, J. H. Smet, V. Umansky and K. von Klitzing Phys. Rev. B **71**, 201306(R) (2005).

[50] L.B. Rigal, et al. Phys. Rev. Lett. **82**, 1249 (1999)

[51] J. Alicea, L. Balents, M.P.A. Fisher, A. Paramekanti, L. Radzihovsky, Phys. Rev. B **71**, 235322 (2005)

[52] V. I Belinicher, and B. I. Sturman, Sov. Phys. Usp. **23**, 199 (1980).

[53] B. J. van Wees, L. P. Kouwenhoven, and C. J. P. M. Harmans, *et al*, Phys. Rev. Lett. **62** 2523(1989)